APPLIED PHYSICS REVIEWS—FOCUSED REVIEW

Electromechanical phenomena in semiconductor nanostructures

L. C. Lew Yan Voon[1,a)] and M. Willatzen[2]
[1]*Department of Physics, Wright State University, 3640 Colonel Glenn Hwy, Dayton, Ohio 45435, USA*
[2]*Mads Clausen Institute, University of Southern Denmark, Alsion 2, DK-6400 Sønderborg, Denmark*

(Received 12 July 2010; accepted 3 December 2010; published online 9 February 2011)

Electromechanical phenomena in semiconductors are still poorly studied from a fundamental and an applied science perspective, even though significant strides have been made in the last decade or so. Indeed, most current electromechanical devices are based on ferroelectric oxides. Yet, the importance of the effect in certain semiconductors is being increasingly recognized. For instance, the magnitude of the electric field in an AlN/GaN nanostructure can reach 1–10 MV/cm. In fact, the basic functioning of an (0001) AlGaN/GaN high electron mobility transistor is due to the two-dimensional electron gas formed at the material interface by the polarization fields. The goal of this review is to inform the reader of some of the recent developments in the field for nanostructures and to point out still open questions. Examples of recent work that involves the piezoelectric and pyroelectric effects in semiconductors include: the study of the optoelectronic properties of III-nitrides quantum wells and dots, the current controversy regarding the importance of the nonlinear piezoelectric effect, energy harvesting using ZnO nanowires as a piezoelectric nanogenerator, the use of piezoelectric materials in surface acoustic wave devices, and the appropriateness of various models for analyzing electromechanical effects. Piezoelectric materials such as GaN and ZnO are gaining more and more importance for energy-related applications; examples include high-brightness light-emitting diodes for white lighting, high-electron mobility transistors, and nanogenerators. Indeed, it remains to be demonstrated whether these materials could be the ideal multifunctional materials. The solutions to these and other related problems will not only lead to a better understanding of the basic physics of these materials, but will validate new characterization tools, and advance the development of new and better devices. We will restrict ourselves to nanostructures in the current article even though the measurements and calculations of the bulk electromechanical coefficients remain challenging. Much of the literature has focused on InGaN/GaN, AlGaN/GaN, ZnMgO/ZnO, and ZnCdO/ZnO quantum wells, and InAs/GaAs and AlGaN/AlN quantum dots for their optoelectronic properties; and work on the bending of nanowires have been mostly for GaN and ZnO nanowires. We hope the present review article will stimulate further research into the field of electromechanical phenomena and help in the development of applications. [doi:10.1063/1.3533402]

TABLE OF CONTENTS

a)Electronic mail: lok.lewyanvoon@wright.edu.

I. INTRODUCTION

A. Piezoelectricity

The best known form of electromechanical coupling is the piezoelectric effect, though there are other effects such as electrostriction and pyroelectricity. The origin of piezoelectricity is attributed to the discovery in 1880 by Pierre and Jacques Curie that certain crystals develop opposite charges on their surfaces when pressure is applied.[1] The experiments involved flat plates with metal electrodes connected to an electrometer; they studied numerous crystals including quartz, Rochelle salt and zinc blende.

According to Cady,[1] a precise definition of piezoelectricity is "electric polarization produced by mechanical strain in crystals belonging to certain classes, the polarization being proportional to the strain and changing sign with it." This is also known as the direct effect; the converse effect is when a crystal is strained when an electric field is applied:

$$P_i = e_{ijk} S_{jk} \quad \text{(direct)}, \tag{1}$$

$$S_{ij} = d_{ijk} P_k \quad \text{(converse)}, \tag{2}$$

where **P** is the polarization, S the strain tensor, and e and d are the piezoelectric coefficients. The phenomenon is, in fact, reversible and neither of the direct nor converse effect is more fundamental; the naming is historical. Electrostriction is defined as a deformation produced by electric stress; it differs from the converse effect in being proportional to the square of the applied electric field.

Analysis of the various effects requires piezoelectric constitutive laws which can be obtained from differential expressions in the total free energy and related thermodynamic potentials. The application of thermodynamic principles was carried out by Lippmann just a year after the discovery of piezoelectricity.[1] For a dielectric, the total internal energy change reads:

$$dU = dU^{\text{mech.}} + dU^{\text{elec.}} = \Theta d\sigma + T_{ik} dS_{ik} + E_i dD_i, \tag{3}$$

where Θ is the temperature, σ the entropy, T_{ik} the stress, **E** the electric field, and **D** the electric displacement. It is convenient to introduce the electric enthalpy:

$$H^{\text{elec}} = U - E_i D_i, \tag{4}$$

satisfying the differential expression

$$dH^{\text{elec}} = \Theta d\sigma + T_{ik} dS_{ik} - D_i dE_i. \tag{5}$$

Applying the chain rule to derivatives of the electric potential H^{elec} leads to the identity relation

$$e_{ikl} = \left(\frac{\partial D_i}{\partial S_{kl}}\right)_E = -\left(\frac{\partial^2 H^{\text{elec}}}{\partial S_{kl}\,\partial E_i}\right) = -\left(\frac{\partial^2 H^{\text{elec}}}{\partial E_i\,\partial S_{kl}}\right) = -\left(\frac{\partial T_{kl}}{\partial E_i}\right)_S. \tag{6}$$

We also have the electric and elastic coefficients:

$$\epsilon_{ik}^{T(S)} = \left(\frac{\partial D_i}{\partial E_k}\right)_{T(S)} \quad \text{(permittivity tensor)}, \tag{7}$$

$$c_{klmn}^{D(E)} = \left(\frac{\partial T_{kl}}{\partial S_{mn}}\right)_{D(E)} \quad \text{(stiffness tensor)}, \tag{8}$$

where superindices refer to quantities kept constant under differentiation. If, in the absence of strain and electric field, stress is zero and a remnant spontaneous polarization contribution, P^{sp}, to the electric displacement exists, the following isentropic expressions apply:

$$D_i = P_i^{\text{sp}} + \left(\frac{\partial D_i}{\partial E_k}\right)_S E_k + \left(\frac{\partial D_i}{\partial S_{kl}}\right)_E S_{kl} = P_i^{\text{sp}} + \epsilon_{ik}^S E_k + e_{ikl} S_{kl}, \tag{9}$$

$$T_{kl} = \left(\frac{\partial T_{kl}}{\partial E_i}\right)_S E_i + \left(\frac{\partial T_{kl}}{\partial S_{mn}}\right)_E S_{mn} = -e_{ikl} E_i + c_{klmn}^E S_{mn}. \tag{10}$$

The latter equations will form much of the analysis of electromechanical effects in semiconductors.

B. Second-order piezoelectricity

Recent calculations by Bester *et al.*[2,3] seem to indicate that second-order piezoelectricity, associated with the second term in the equation,

$$P_i = e_{ijk} S_{jk} + \frac{1}{2} \sum_{jklm} B_{ijklm} S_{jk} S_{lm}, \tag{11}$$

is important for zincblende (ZB) nanostructures.

C. Electrostriction

Newnham *et al.*[4] define it as the quadratic coupling between strain and electric field:

$$S_{ij} = Q_{ijkl} P_k P_l = M_{ijkl} E_k E_l. \tag{12}$$

It is characterized by a tensor property of even rank, as opposed to piezoelectricity which is given by a polar tensor. Thus, electrostriction is possible in centrosymmetric crystals such as silicon.

The constitutive relations can be obtained from the Gibbs function:

$$S_I = M_{Iij} E_i E_j + s_{IJ} T_J + d_{iI} E_i, \quad \text{direct}, \tag{13}$$

$$D_i = (\epsilon_{ij} + M_{Iij} T_I) E_j + d_{iI} T_I, \quad \text{converse}, \tag{14}$$

and s_{IJ} is the compliance tensor. In the expressions above, capital subscripts I,J are Voigt indices and run from 1 to 6 (1,…,6 corresponding to xx, yy, zz, yz, xz, xy, respectively)

and small subscripts i,j are Cartesian and run from 1 to 3; this also explains why M, s, and d here are characterized by three, two, and two subscripts, respectively.

II. ELECTROMECHANICAL COEFFICIENTS IN CRYSTALS

Having defined the electromechanical coefficients, we now look at their forms for certain crystals of relevance to the nanostructures.

A. Piezoelectricity

Voigt provided a symmetry analysis to identify which piezoelectric components are nonzero for which crystal class. The key property of the piezoelectric effect is that the sign of the response changes with the sign change in the cause. This differentiates it from, e.g., electrostriction. Furthermore, it points to some preferred direction, or polarity, in the internal structure. There are 20 crystal classes with an absence of inversion.

The phenomenon couples the electic and elastic behaviors. Given that the stress tensor has 6 components and the electric field has 3, there are up to 18 piezoelectric coefficients for an arbitrary crystal. The general expressions obtained above can be significantly simplified in the case of crystal structures using group theory. Two crystal structures where piezoelectric effects exist of importance to semiconductors are the ZB cubic and wurtzite (WZ) hexagonal systems. The general tensor form of $\epsilon_{ik}^S, e_{ikl}, c_{klmn}^E$ for ZB and WZ will be given next and briefly explained.

1. ZB

Tetragonal symmetry and symmetry rotations through $\pi/2$ about the x and y axes show that only three independent stiffness coefficients exist in cubic systems.[5] Thus, one may write for the stiffness tensor using Voigt notation:

$$[c] = [c_{IJ}] = \begin{bmatrix} c_{11} & c_{12} & c_{12} & 0 & 0 & 0 \\ c_{12} & c_{11} & c_{12} & 0 & 0 & 0 \\ c_{12} & c_{12} & c_{11} & 0 & 0 & 0 \\ 0 & 0 & 0 & c_{44} & 0 & 0 \\ 0 & 0 & 0 & 0 & c_{44} & 0 \\ 0 & 0 & 0 & 0 & 0 & c_{44} \end{bmatrix}. \tag{15}$$

In obtaining the stiffness tensor, we employed the expression

$$T_{ij} = \frac{\partial F}{\partial S_{ij}} = c_{ijkl} S_{kl}, \tag{16}$$

where F is the free energy. The symmetry operations used in obtaining the general structure of the stiffness tensor above do not encompass the inversion operator. Hence, the above form applies to ZB as well. We note in passing that for an isotropic solid, the same structure of the stiffness tensor is obtained, except that the higher symmetry imposes the following condition:

$$c_{44} = \frac{1}{2}(c_{11} - c_{12}). \tag{17}$$

In a similar way, group theory allows one to find the general form of the ZB permittivity and the piezoelectric e tensor:[6]

$$[\epsilon] = [\epsilon_{ij}] = \begin{bmatrix} \epsilon_{11} & 0 & 0 \\ 0 & \epsilon_{11} & 0 \\ 0 & 0 & \epsilon_{11} \end{bmatrix}, \tag{18}$$

$$[e] = [e_{Ij}] = \begin{bmatrix} 0 & 0 & 0 \\ 0 & 0 & 0 \\ 0 & 0 & 0 \\ e_{14} & 0 & 0 \\ 0 & e_{14} & 0 \\ 0 & 0 & e_{14} \end{bmatrix}. \tag{19}$$

We emphasize that lack of inversion symmetry in ZB is required for a nonvanishing piezoelectric e tensor as it is a tensor of odd rank.

2. WZ

Hexagonal structures belong to the class C_6 and one often chooses the sixfold rotational axis to be the z axis. The stiffness tensor has the form

$$[c] = \begin{bmatrix} c_{11} & c_{12} & c_{13} & 0 & 0 & 0 \\ c_{12} & c_{11} & c_{13} & 0 & 0 & 0 \\ c_{13} & c_{13} & c_{33} & 0 & 0 & 0 \\ 0 & 0 & 0 & c_{44} & 0 & 0 \\ 0 & 0 & 0 & 0 & c_{44} & 0 \\ 0 & 0 & 0 & 0 & 0 & \frac{1}{2}(c_{11} - c_{12}) \end{bmatrix}, \tag{20}$$

again using Voigt notation.[6] As before, the symmetry operations used in obtaining the general structure of the stiffness tensor do not encompass the inversion operator and, hence, the above tensor form applies to WZ as well.

Similarly, group theory allows one to find the general form of the WZ permittivity and piezoelectric e tensor:[6]

$$[\epsilon] = \begin{bmatrix} \epsilon_{11} & 0 & 0 \\ 0 & \epsilon_{11} & 0 \\ 0 & 0 & \epsilon_{33} \end{bmatrix}, \tag{21}$$

$$[e] = \begin{bmatrix} 0 & 0 & e_{31} \\ 0 & 0 & e_{31} \\ 0 & 0 & e_{33} \\ 0 & e_{15} & 0 \\ e_{15} & 0 & 0 \\ 0 & 0 & 0 \end{bmatrix}. \tag{22}$$

There are, thus, three independent piezoelectric coefficients for WZ.

3. Measurements and calculations

Typically, the techniques for obtaining the electromechanical constants rely either on the direct or converse effect, though a few are indirect. Examples include, for piezoelec-

TABLE I. Representative values of piezoelectric coefficients and spontaneous polarization from the literature. e_{14} is for the ZB structure and the rest is for the WZ structure. All data are taken from Bernardini *et al.* (Ref. 41) except for those of MgO and CdO taken from Gopal and Spaldin (Ref. 47).

	e_{14}	e_{33}	e_{31}	e_{15}	P^{sp}
		(Cm^{-2})			
AlAs	−0.017				
GaAs	−0.104				
InAs	−0.017				
AlP	0.035				
GaP	−0.052				
InP	0.035				
AlN		1.46	−0.60	⋯	−0.081
GaN		0.73	−0.49	⋯	−0.029
InN		0.97	−0.57	⋯	−0.032
MgO		2.26	−0.38		
BeO		0.02	−0.02	⋯	−0.045
ZnO		0.89	−0.51	⋯	−0.057
CdO		1.67	−0.48		

tricity, resonance methods,[7] the attenuation of ultrasonic shear wave propagation,[8] an interferometric direct method,[9,10] piezoresponse force microscopy (PFM),[11–13] and a cantilever-based direct method.[14] Uncertainty quoted for bulk materials can be as high as 10%.[9] Difficulties associated with a quantitative measurement using the PFM method have been discussed.[13,15–18] All-electrical techniques for measuring piezoelectric displacements have been developed.[19]

Within the appropriate model of electromechanical interaction, piezoelectric coefficients can also be extracted from analyzing the optoelectronic properties of the semiconductor heterostructures. This technique is fraught with uncertainties since it requires an accurate knowledge of the structure and an accurate theory of the electronic properties. Nevertheless, this technique has been widely used on III-nitrides quantum wells (QWs). We refer the reader to the review by Feneberg and Thonke[20] for a detailed discussion of this approach.

Formal expressions for the bulk piezoelectric coefficients go back as far as the work of Born published in 1915 and later[21–24] and of Huang.[25,26] Calculations of the piezoelectric coefficients using microscopic models have been carried out.[2,7,27–52] These expressions can be classified into model, traditional first-principles, and Berry-phase first-principles calculations. The modern theory of polarization in dielectrics[53] appears to have first been used to calculate piezoelectric coefficients in 1994.[39] In spite of the apparent good agreement with experimental data, it should be emphasized that the piezoelectric coefficient results from the difference of two important contributions and is, therefore, not a trivial calculation. Indeed, work by Noel *et al.*[45] has shown how different computational parameters can change the results by up to 30% for ZnO. Zheng *et al.*[50] even believe an accuracy of only 10%–40% is appropriate. An alternative formulation has recently been used to compute the piezoelectric coefficients.[54,55] This is a hybrid of the model and first-principles approaches, whereby the polarization is written in terms of microscopic parameters such as the effective charge and bond polarity using the Harrison bond-orbital model, and the latter parameters are computed from first-principles.

TABLE II. Quadratic piezoelectric coefficients (C/m^2).

	B_{114}	B_{124}	B_{156}
InAs[a]	−0.531	−4.076	−0.120
GaAs[a]	−0.439	−3.765	−0.492
GaP[b]	−0.762	−3.562	−0.975

[a]Reference 2.
[b]Reference 56.

A few theoretical values of the piezoelectric coefficients are given in Table I. There is quite a spread among reported values so far and we have avoided to give a listing of all published values. For the WZ nitrides, Feneberg and Thonke[20] have provided a fairly extensive listing of values. Note that e_{15} values have generally not been computed.

B. Second-order piezoelectricity

It follows from symmetry considerations that the number of free second-order piezoelectric B_{ijklm} tensor components is three ($B_{xxxyz}=B_{114}, B_{xyyyz}=B_{124}, B_{xxzxy}=B_{156}$) for ZB and eight for WZ ($B_{zzzzz}, B_{zzz\xi\eta}, B_{zz\xi z\eta}, B_{z\xi\eta\xi}, B_{z\xi\xi\eta\eta}, B_{\xi zzz\eta}, B_{\xi\xi z\eta\eta}, B_{\xi\eta z\xi\eta}$).

Values of the second-order piezoelectric coefficients have been computed using density-functional theory (DFT) (VASP and ABINIT) for a few ZB materials (Table II).

C. Electrostriction

The symmetry properties of the electrostriction M_{ijkl} tensor are equivalent to the symmetry properties of the stiffness tensor c_{ijkl}. Hence, the number of free M_{ijkl} parameters is three ($M_{1111}, M_{1122}, M_{2323}$) for ZB and five for WZ ($M_{1111}, M_{1122}, M_{1133}, M_{3333}, M_{2323}$).

While electrostriction has been investigated for a long time, there are only a handful of measurements for the tetrahedral semiconductors, namely for Si, diamond,[57] AlN,[4] MgO,[4] and GaN (Ref. 58) (Table III). For the WZ semiconductors, experimentally reported values of the electrostrictive coefficients for AlN and GaN differ by three orders of magnitude.[4,58] Our recent calculations would indicate that the experimental values for GaN and AlN are in error.[59]

Electrostrictive measurements require a very delicate instrument since the effect can be very small. For example, a field of 1 MV m^{-1} only produces a strain of the order of 10^{-9}; for a 1 mm thick sample, this translates to a displace-

TABLE III. M_{33} (in 10^{-22} m^2 V^{-2}) coefficients: calculated and experimental.

	C	GaN	AlN	ZnO	MgO
Calc. (Ref. 59)		1.0	−1.3	−3.6	12.6
Expt.	0.28 (Ref. 57)	1200 (Ref. 58)	14.6 (Ref. 4)	⋯	8.26 (Ref. 4)

ment of 0.01 Å.[4] The minute displacements are typically measured using a laser dilatometer based on Michelson interferometry.[4,57,58] A nice but dated review article is by Newnham.[4]

III. ELECTROMECHANICAL EFFECTS IN SEMICONDUCTOR NANOSTRUCTURES

This constitutes the main section of the present review article. The basic message is that electromechanical coupling is fundamental in determining the electronic, mechanical, and optical properties of nanostructures made of piezoelectric materials. In particular, electromechanical effects and strain effects play a dominant role in determining electronic band structures, wave functions, and optoelectronic properties of semiconductor nanostructures. In addition, they also lead to the coupling between vibrations and electricity generation in nanowires.

Two types of devices have already been commercialized, both of the QW type and both using III-V nitrides. One is a transistor structure, typically made out of GaN/AlGaN multilayers. The other is a laser structure, already realized with InGaN/GaN multilayers. Still very much under research are ZB and WZ quantum dots (QDs) and nanowires. In all of the above, the relevance of the electromechanical effect is due to either built-in strain between different materials or the mechanical bending of the nanostructures leading to a so-called internal polarization field. For the laser structures, this could, in fact, be detrimental to the efficient operation of the device since the field would typically separate the charges. For the vibrating nanowires, the electromechanical effect is inherent to their operation as energy harvesters. Experimentally, the question is how is the electromechanical effect identified and measured. Invariably though, the analysis of the experimental data requires some theoretical modeling in order to deduce either the electromechanical fields or the electromechanical coefficients. Hence, we focus on presenting the theoretical picture and relate to some experimental data for comparison. Theoretically, there have been studies of the correct framework for analyzing the effect as well as the actual origin of the electric field (e.g., whether from linear or nonlinear electromechanical effects), the impact of charge carriers on the effect, and the importance of the effect for various nanostructures and materials. These topics are now discussed.

A. Theoretical framework

In the following, for concreteness, we will restrict to the piezoelectric effect and give the equations for a QW structure; extensions will be discussed where relevant. The electromechanical problem is the study of the solution to the coupled Schrödinger–Poisson–Navier equations. For a doped semiconductor, one can write

$$\mathbf{T} = \mathbf{cS} - \mathbf{eE}, \tag{23}$$

$$\mathbf{D} = \epsilon\mathbf{E} + \mathbf{P}^{\mathrm{sp}} + \mathbf{eS}, \tag{24}$$

$$\nabla \cdot \mathbf{T} = \rho_d \frac{\partial^2 \mathbf{u}}{\partial t^2}, \tag{25}$$

$$\nabla \cdot \mathbf{D} = e[N - n(\mathbf{r})], \tag{26}$$

$$H\Psi = E\Psi, \tag{27}$$

with

$$n(z) = 2\sum_{j=0}^{N} \int\int \frac{L_x L_y}{(2\pi)^2} |\Psi^{(j)}(z)|^2 f(E^{(j)}, E_F) dk_x dk_y, \tag{28}$$

$$f(E^{(j)}) = \left[1 + \exp\left(\frac{E^{(j)} - E_F}{k_B T}\right)\right]^{-1}, \tag{29}$$

$$H = H_0(-i\nabla) + H_c + H_s - e\phi, \tag{30}$$

where Eq. (23) is the converse effect, Eq. (24) is the direct effect, Eq. (25) is the Navier equation with the displacement $\mathbf{u}$ and mass density ρ_d, Eq. (26) is the Poisson equation with N the impurity concentration, and Eq. (27) is Schrödinger's equation. $n(z)$ is the free-carrier density at a finite temperature T, $f(E)$ the Fermi–Dirac function, E_F is the Fermi level, and the Hamiltonian H consists of the band term H_0, a band offset between dissimilar materials H_c, a deformation potential H_s due to strain, and an electrostatic potential $-e\phi$ due to the charge carriers and piezoelectric effect. The Hamiltonian is given in an envelope-function form, which is the approach used by most, though alternative formulations such as with a tight-binding Hamiltonian has been used.

All of the above equations taken together is a nonlinear coupled problem. Nevertheless, it has been the practice to treat the problem in two parts. One involves just solving Eqs. (23)–(25), which is the pure electromechanical problem giving the self-consistent strain and electric fields. For simple cases, analytic solutions can even be obtained. Initial attempts have also solved the equations nonself-consistently, which implies dropping the electric-field term in Eq. (23); this is known as the semicoupled model. The validity or not of the latter approximation has now been extensively studied both in one-dimensional (1D) and in three-dimensional (3D),[60–63] and the results have been shown to depend upon the material system. The other approach is to solve the full set of equations, again with the possibility of dropping some of the coupling terms. One is then typically interested in the impact of the electromechanical coupling on the electronic properties.

The above framework has been applied to various material systems and nanostructures. A survey of the relevant literature is now provided.

B. Electromechanical fields in ZB nanostructures

Almost all of the work so far has been for the InAs/GaAs material system. From Table I, it can be seen that GaAs has the largest (in magnitude) e_{14} and InAs has one of the smallest e_{14} of the common semiconductors.

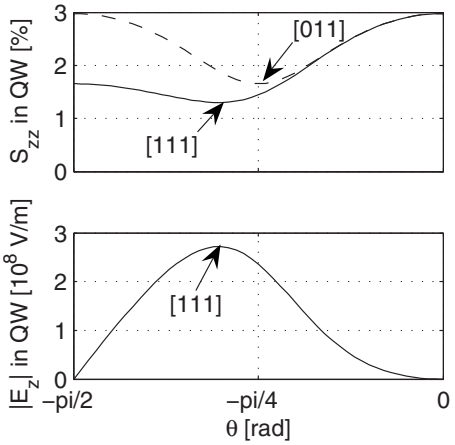

FIG. 1. Strain and electric field in a ZB AlN/GaN QW. Reprinted with permission from L. Duggen, M. Willatzen, and B. Lassen, Phys. Rev. B **78**, 205323 (2008). ©2008, American Physical Society.

1. QWs

The effect of piezoelectricity was, indeed, first studied for ZB QWs by Smith in 1986.[64] Piezoelectric fields exist in ZB QWs grown along any direction other than [001].[65] Since there is only one nonzero piezoelectric coefficient for ZB, e_{14}, a polarization is generated from an off-diagonal strain:

$$P_i = 2e_{14}S_{jk}. \tag{31}$$

For a [111] heterostructure, the piezoelectric fields are also in the [111] direction.

Smith and Mailhiot[65] derived the most general expression for the induced polarization for a bilayer superlattice (SL) for an arbitrary growth direction by minimizing the strain energy for the strain tensor and using the semicoupled formalism. The polarization is uniform within each layer but reverses direction in the two layers due to the different sign of the strain tensor. Hence, the divergence of polarization at the interfaces leads to an internal longitudinal electric field for growth directions other than [001] and [110]. For example, for a [111]-grown III-V SL with a negative e_{14}, the layer with the larger lattice constant has a polarization vector pointing from the cation (A face) to the anion (B face).[64] They found that, for a GaAs–$In_{0.2}Ga_{0.8}As$ SL with a 1.4% lattice mismatch, the maximum electric field is around 0.15 MV/cm for a [111] SL; this corresponds to an interface charge of 2×10^{12} e/cm^2. Experimentally a field of ~0.5 MV/cm was measured for CdTe/CdMgTe QWs.[66] A more recent calculation for a ZB AlN/GaN QW is shown in Fig. 1. The orientational dependence is similar to the earlier case of GaAs–$In_{0.2}Ga_{0.8}As$ SL (Ref. 65) but the electric field is larger by an order of magnitude. Duggen *et al.*[67] also compared the semicoupled and the fully-coupled models (Table IV) and found the differences to be negligible for InGaAs/GaAs but to be up to about 10% for AlN/GaN. In Table IV, S'_{zz} strain contributions due to lattice mismatch ($S_{\text{semicoupled}}$) and piezoelectric effects (S_{coupled}) are given for QW ZB structures (the subscript z in S'_{zz} refers to the growth direction [111].[67] The total strain,

$$S_{\text{fully-coupled}} = S_{\text{semicoupled}} + S_{\text{coupled}}, \tag{32}$$

for the S'_{zz} component can be written as

$$S'_{zz} = \frac{3(c_{11}^{(2)} + 2c_{12}^{(2)})a_{\text{mis}}}{4\dfrac{e_{x4}^{(2)_2}}{\epsilon^{(2)}} + c_{11}^{(2)} + 2c_{12}^{(2)} + 4c_{44}^{(2)}} - a_{\text{mis}}, \tag{33}$$

where the superscript (2) refers to the QW layer and a_{mis} is the lattice mismatch. It is clear from Table IV that piezoelectric effects contribute to the total strain by a (negligible) amount (less than 1% relative strain change) for GaAs/$In_xGa_{1-x}As$ ZB structures while, for nitride-based ZB structures (AlN/GaN, GaN/InGaN, GaN/AlN), the contribution is small but noticeable (up to approximately 10% relative strain change). It should be mentioned that piezoelectric effects do not contribute to strain for [001]-grown ZB QW structures in contrast to the corresponding WZ result.

Since there is no direct measurement of either the piezoelectric coefficient or of the piezoelectric field, the correlation of measured data to the piezoelectric coefficients is complicated. It has been reported that measurements of the piezoelectric field in InGaAs QWs lead to e_{14} values for the alloy that are about 35% smaller than the values obtained by linear interpolation of accepted values for InAs and GaAs.[2,70] Bester *et al.* found that a second-order nonlinear piezoelectric contribution they computed leads to very different internal fields [Fig. 2(a)] and could account for the discrepancy. The second-order nonlinear piezoelectric coefficients they found using DFT are given in Table II. Indeed, Lepkowski[77] carried out a more detailed study and showed that, e.g., for a 10 nm $In_{0.15}Ga_{0.85}As$/15 nm GaAs multiple QW, the nonlinear (linear) theory gives an internal electric field of 166

TABLE IV. Contributions to S'_{zz} in the [111]-grown QW layer for different material compositions corresponding to open-circuit conditions. For GaAs/$In_xGa_{1-x}As$, both $E'_{z,t}$ and $E'_{z,e}$, being the theoretical and the experimental electric field in the QW layer, respectively, are listed for comparison.

Substrate/QW	S_{semi} (%)	S_{coupling} (%)	Deviation (%)	$E'_{z,t}$ (V/μm)	$E'_{z,e}$ (V/μm)
GaAs/$In_{0.1}Ga_{0.9}As$	0.34	−0.002	0.5	15.56	17 ± 1 [a]
GaAs/$In_{0.2}Ga_{0.8}As$	0.710	−0.003	0.4	28.63	25[b]
AlN/GaN	1.34	−0.04	3.1	271.6	
GaN/$In_{0.3}Ga_{0.7}N$	1.69	−0.07	4.4	355.0	
GaN/InN	7.24	−0.61	−9.1	1441.5	
GaN/AlN	−0.91	0.04	−4.7	−280.3	

[a]Reference 68.
[b]Reference 69.

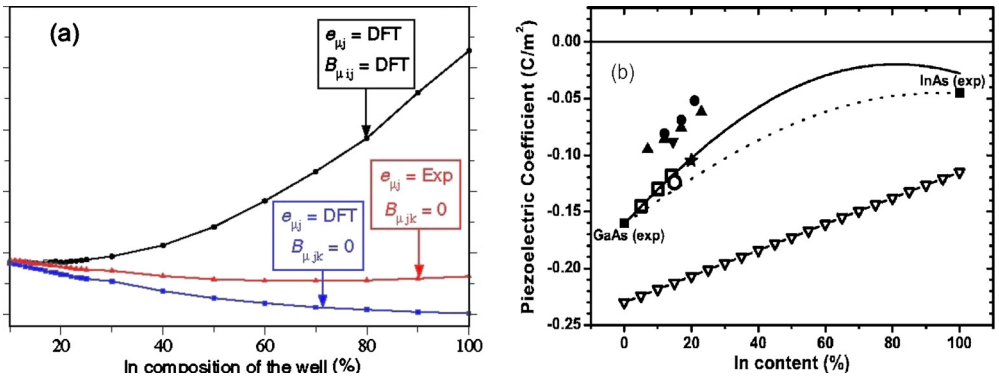

FIG. 2. (Color online) (a) Piezoelectric field as a function of In composition x. Circles: calculations using DFT computed linear (e) and nonlinear piezoelectric (B) coefficients. Reprinted with permission from Ref. 2. (b) Piezoelectric coefficient as a function of In composition x. Hollow squares (theory) are from Ref. 54, hollow circle from Ref. 70, upside-down triangles from Ref. 71, triangles from Ref. 72, star from Ref. 73, filled circles from Refs. 74–76. Reprinted with permission from M. A. Miglionato, D. Powell, A. G. Cullis, T. Hammerschmidt, and G. P. Srivastava, Phys. Rev. B **74**, 245332 (2006). ©2006, American Physical Society.

kV/cm (137 kV/cm), to be compared with the experimental value extracted from optical measurements of 165 kV/cm if In segregation is ignored.[70] It has been pointed out that the latter value is, however, obtained by extracting an electric field using a linear theory for a single QW; hence, the apparent agreement is not necessarily conclusive. An alternate explanation in terms of the strain dependence of the linear piezoelectric coefficients has been proposed[54] [Fig. 2(b), hollow square] and shown to be in good agreement with the one experimental data provided (hollow circle). They also deduced that the parameters of Bester *et al.* should really give a field of 80 kV/cm and not the 166 kV/cm reported in Ref. 77. There is clearly disagreement in the literature regarding this issue. One approach to determining the correct theory is to study nonalloyed layers. Nonetheless, currently, it appears that the issue of a quantitative agreement between theory and experiment is far from having been achieved.

2. QDs

Piezoelectric fields in QDs have also been studied.[3,56,78–88] The strain problem is solved either using a continuum elasticity model or is atomistic based. Numerical techniques for solving for the strain and polarization fields have included valence-force field coupled with finite difference,[83] finite-element,[89] Green's function,[81,90] and image-potential[91] based methods. Most calculations have been based on the semicoupled model except for those of Pan and co-workers[81,82] and our work.[92]

There are, of course, very few analytical results for a 3D nanostructure. Davies[79] did obtain an expression for the piezoelectric potential outside of a spherical InAs QD in an infinite GaAs matrix:

$$V(\mathbf{r}) = -\frac{3e_{14}\delta a}{\varepsilon_0\varepsilon_r}\frac{1+\nu}{1-\nu}\left(\frac{a}{r}\right)^2\left[1-\left(\frac{a}{r}\right)^2\right]\frac{xyz}{r^3}, \tag{34}$$

where δ is the lattice mismatch (7.2% for InAs/GaAs), a is the dot radius, ε_r is the relative permittivity, and ν the Poisson ratio. Within the isotropic elasticity approximation used, there is no piezoelectric potential inside the spherical dot and the magnitude outside for a 6 nm InAs QD was found to be up to 0.17 V (Fig. 3). For a nonspherical dot, the potential in the InAs region can be expected to be of the order of tens of millielectron volt since e_{14} for InAs is about a quarter of that of GaAs. The potential scales with the dot size[78] as is evident in Eq. (34). Basically all calculations have been done using linear piezoelectricity. Bester *et al.*[3] have recently questioned this. They found that the linear and nonlinear piezoelectric contributions nearly cancel each other out for an InAs/GaAs QD. In fact, they went as far as to conclude that a calculation without the piezoelectric effect is more accurate than one with only the linear term. However, there has been no further study of this issue.

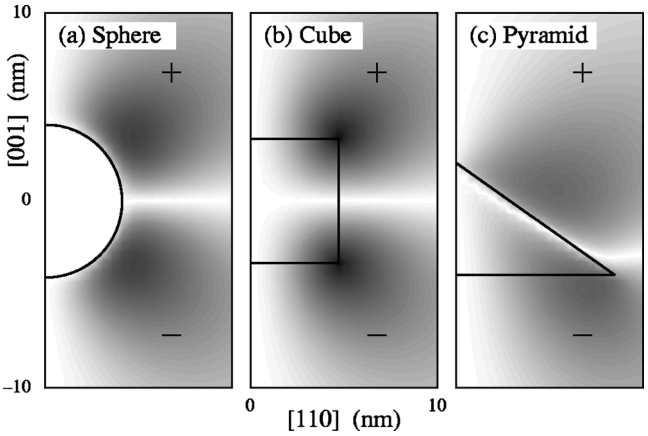

FIG. 3. Piezoelectric potential for dots. Reprinted with permission from J. H. Davies, J. Appl. Phys. **84**, 1358 (1998). ©1998, American Institute of Physics..

C. Electromechanical fields in WZ heterostructures

We next discuss the polarization fields in WZ heterostructures. One major difference compared to ZB is that there are now three distinct piezoelectric coefficients in the bulk. A direct consequence is the existence of a piezoelectric effect even for nanostructures oriented in the (0001) direction. The other major difference is the presence of a spontaneous polarization. Some of the earliest measurements reported internal fields of 1.08 MV/cm in GaN/$In_{0.13}Ga_{0.87}N$ QWs (Ref. 93) and 2.5 MV/cm in GaN/$Al_{0.15}Ga_{0.85}N$ QWs (Ref. 94) both from photoluminescence data, and even of 4.7 MV/cm

(Ref. 95) for GaN on AlN. On the issue of how to calculate the polarization fields, there were apparently conflicting results regarding the need for a fully-coupled model even for QW structures.[60,62] Thus, Jogai *et al.*[60] argued that the internal electric field can be as high as 5 MV/cm for AlGaN/GaN and, consequently, the difference between a full-coupled model and a semicoupled model can be as high as 60%. On the other hand, calculations by Christmas *et al.*[62] found only a 2% error in the internal fields for InGaN/GaN. The discrepancies were explained in terms of the interplay between piezoelectric and spontaneous polarizations.[63]

1. QWs

The first consideration of such effects for WZ nanostructures was probably in 1993 for an (0001) GaN–AlN–GaN structure[96] and it was shown how the stress-induced carrier densities affect the capacitance-voltage characteristics. However, their analysis was only semicoupled and they did not include the effect of spontaneous polarization. Within such an approximation, the polarization in the AlN layer (with smaller lattice constant) takes a particularly simple form:[96]

$$P_z = 2d_{31}(c_{11} + c_{12} - 2c_{13}^2/c_{33})S_{xx}, \tag{35}$$

with the polarization pointing from the anion (B) face to the cation (A) face. From Table I, if the lattice mismatch is about the same, then one can expect the electric field to be a few times larger for the GaN/AlN system compared to the InGaAs/GaAs one.

Soon after the first calculations of spontaneous polarization,[41] it was realized that they can be important in the nanostructures[97] as, by themselves, they can lead to electric fields of the order of megavolt per centimeter. The direction of piezoelectric and spontaneous polarizations are given in Fig. 4. For a GaN/AlGaN QW along [0001] with well width $L_W \ll$ barrier width L_B (i.e., only the GaN layer is strained), a simple expression for the polarization and electric fields can be written down using the semicoupled model:[98]

$$P^{\mathrm{PE}} = 2\frac{a_{\mathrm{AlGaN}} - a_{\mathrm{GaN}}}{a_{\mathrm{GaN}}}\left(e_{31} - e_{33}\frac{c_{13}}{c_{33}}\right), \tag{36}$$

$$E_W = \frac{P^{\mathrm{SP}}_{\mathrm{AlGaN}} - P^{\mathrm{SP}}_{\mathrm{GaN}} - P^{\mathrm{PE}}_{\mathrm{GaN}}}{\varepsilon_0(\epsilon_W + \epsilon_B L_W/2L_B)}, \tag{37}$$

$$E_B = \frac{P^{\mathrm{SP}}_{\mathrm{GaN}} - P^{\mathrm{PE}}_{\mathrm{GaN}} - P^{\mathrm{SP}}_{\mathrm{AlGaN}}}{\varepsilon_0(\epsilon_B + \epsilon_W L_B/2L_W)}. \tag{38}$$

We note, however, that if one performs the appropriate fully-coupled calculation, the actual strain would be different from the lattice mismatch.[63,99] The analytic solution for a strained (0001) QW grown on a substrate (Fig. 5) using the fully-coupled model has been given.[63] The study of the coupling of electrostatic and mechanical fields requires solving Eqs. (23)–(26). The strain **S** accounts for the lattice mismatch and is defined by:[63,100]

$$S_1 = \frac{\partial u_x}{\partial x} - \frac{a(\mathbf{r}) - a^{(1)}}{a^{(1)}}, \quad S_4 = \frac{1}{2}\left(\frac{\partial u_y}{\partial z} + \frac{\partial u_z}{\partial y}\right),$$

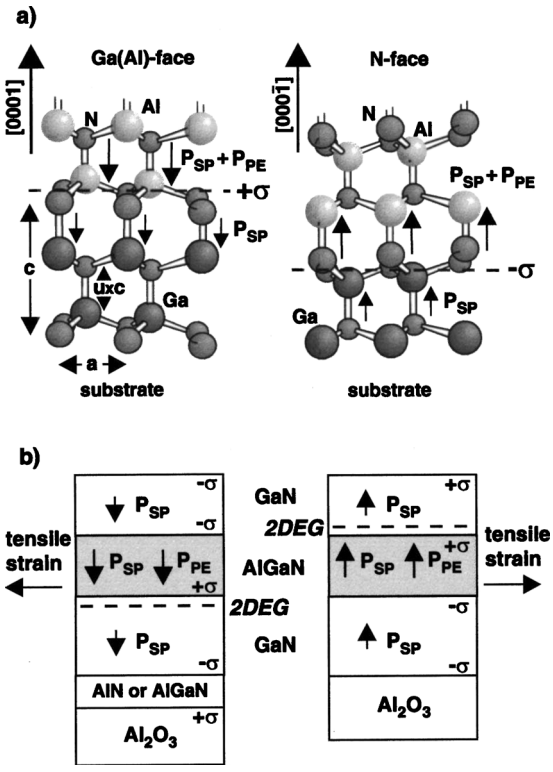

FIG. 4. AlN/GaN heterostructures. (a) Crystal structures. (b) Direction of piezoelectric (PE) and spontaneous (SP) polarizations. Reprinted with permission from O. Ambacher, B. Foutz, J. Smart, J. R. Shealy, N. G. Weimann, K. Chu, M. Murphy, A. J. Sierakowski, W. J. Schaff, L. F. Eastman, R. Dimitrov, A. Mitchell, and M. Stutzmann, , J. Appl. Phys. **87**, 334 (2000). ©2000, American Institute of Physics.

$$S_2 = \frac{\partial u_y}{\partial y} - \frac{a(\mathbf{r}) - a^{(1)}}{a^{(1)}}, \quad S_5 = \frac{1}{2}\left(\frac{\partial u_x}{\partial z} + \frac{\partial u_z}{\partial x}\right),$$

$$S_3 = \frac{\partial u_z}{\partial z} - \frac{c(\mathbf{r}) - c^{(1)}}{c^{(1)}}, \quad S_6 = \frac{1}{2}\left(\frac{\partial u_x}{\partial y} + \frac{\partial u_y}{\partial x}\right), \tag{39}$$

where $a(\mathbf{r})$, $c(\mathbf{r})$ are the lattice constants at position $\mathbf{r}$ while $a^{(1)}$, $c^{(1)}$ denote the lattice constants of the bulk substrate.

The strain along the QW growth direction can be written as:[60,63]

$$S_3 = -\frac{2c_{13}^{(1)}}{c_{33}^{(1)}}S_1 + \left[\frac{2e_{33}^{(1)}(e_{33}^{(1)}c_{13}^{(1)} - e_{13}^{(1)}c_{33}^{(1)})}{c_{33}^{(1)}(\epsilon_{\parallel,1}c_{33}^{(1)} + e_{33}^{(1)2})}\right]S_1 + \frac{e_{33}^{(1)}(P^{\mathrm{sp,GaN}} - P^{\mathrm{sp},1})}{\epsilon_{\parallel,1}c_{33}^{(1)} + e_{33}^{(1)2}} \equiv S_{\mathrm{uncoupled}} + S_{\mathrm{coupled}} + S_{\mathrm{spon}}, \tag{40}$$

where we have labeled the three strain terms according to

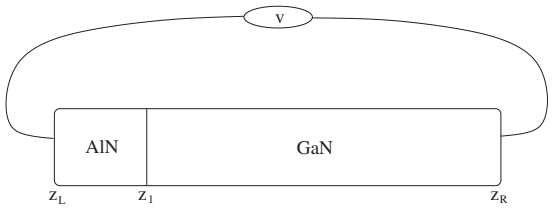

FIG. 5. Schematics of the two-layer HFET structure. Reprinted with permission from M. Willatzen, B. Lassen, and L. C. Lew Yan Voon, J. Appl. Phys. **100**, 124309 (2006). ©2006, American Institute of Physics.

TABLE V. Contributions to the vertical strain in a given layer. The material system: AlN/GaN means GaN is buffer or substrate while AlN is a thin film or QW.[63,101]

	$S_{\text{uncoupled}}$	S_{coupled}	S_{spon}
AlN/GaN	−0.0143	0.0026	0.0026
$Al_{0.3}Ga_{0.7}N/GaN$	−0.0039	0.0004	0.0005
$In_{0.2}Ga_{0.8}N/GaN$	0.0119	−0.0008	0.0001
$ZnO/Zn_{0.8}Mg_{0.2}O$	0.0032	−0.0006	−0.0003

their origin. Equation (40) can be used to understand the relative impact of piezoelectricity, fully-coupled and spontaneous polarization for different material systems.

The relative magnitudes of the three strain contributions are given in Table V for four material compositions: AlN/GaN, $Al_{0.3}Ga_{0.7}N/GaN$, $In_{0.2}Ga_{0.8}N/GaN$, and $ZnO/Zn_{0.8}Mg_{0.2}O$. Table V shows that the relative difference between an uncoupled and a coupled calculation is of order 18%, 9%, 6%, and 20% for AlN, AlGaN, InGaN, and ZnMgO, respectively. Spontaneous polarization adds another 18%, 14%, 0.7%, and 10%. This analysis explains the apparent contradiction between the results of Jogai *et al.*[61] and Christmas *et al.*[62] Thus, the extremely large coupling reported by Jogai *et al.*[61] for AlGaN is here seen to be, in fact, due to both the spontaneous polarization term and the coupling term. For pure AlN, the last two contributions are of equal magnitude if GaN is the substrate, and similarly for ZnO on ZnMgO. For InGaN, the situation is reversed whereby the spontaneous polarization almost does not contribute; hence, the relatively smaller difference in strain reported by Christmas *et al.*[62] is almost entirely due to the difference between the coupled and uncoupled models. Therefore, the relative importance of the fully-coupled model is strongly dependent upon the material system under investigation and spontaneous polarization may or may not be neglected.

The study of polarization fields in II-VI QWs took a little bit more time.[102–106] It was initially expected that the polarization fields for ZnMgO/ZnO QWs would be much smaller than for the nitrides due to the smaller lattice mismatch.[102,103] ZnMgO/ZnO QWs with well width greater than 3 nm were found to have a built-in electric field of about 1 MV/cm.[104] Park and Ahn[105] calculated the internal field in 3 nm $Cd_xZn_{1-x}O/Mg_yZn_{1-y}O$ QWs (Fig. 6). Benharrats *et al.*[106] used their $k\cdot p$ theory in conjunction with the photoluminescence data of Ref. 107 in order to obtain the calculated electric fields given in Fig. 7 (red circles), which they also compared to the calculation of Park and Ahn.[105] They separated out the piezoelectric and spontaneous polarizations and give together with the sheet charge density in Fig. 7(b). Their basic result is that the fields vary linearly with the Cd content, reaching a magnitude of ~3.8 MV/cm for $x=0.2$, a value much larger than for ZnMgO/ZnO QWs.[108]

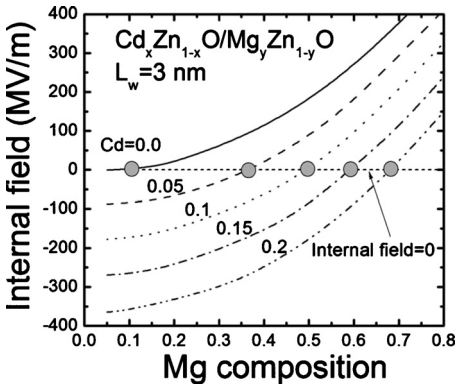

FIG. 6. Internal field for 3 nm $Cd_xZn_{1-x}O/Mg_yZn_{1-y}O$ QWs. Reprinted with permission from S.-H. Park and D. Ahn, Appl. Phys. Lett. **94**, 083507 (2009). ©2009, American Institute of Physics.

The orientational dependence of the piezoelectric effect is much richer for WZ materials. Thus, the piezoelectric field is zero (maximal) for WZ heterostructures grown perpendicular to (along) the c axis. For an intermediate angle, the field may or may not vanish depending upon the combination of piezoelectric parameters.[20] The orientation effect has been more often studied for InGaN/GaN and GaN/AlGaN heterostructures and recently reviewed in Feneberg and Thonke.[20] Park and Ahn found that the internal field is zero for $(11\bar{2}2)$ near the crystal angle of 56^0 independent of the In ratio.[109] For GaN-based QWs, the internal field has been predicted to

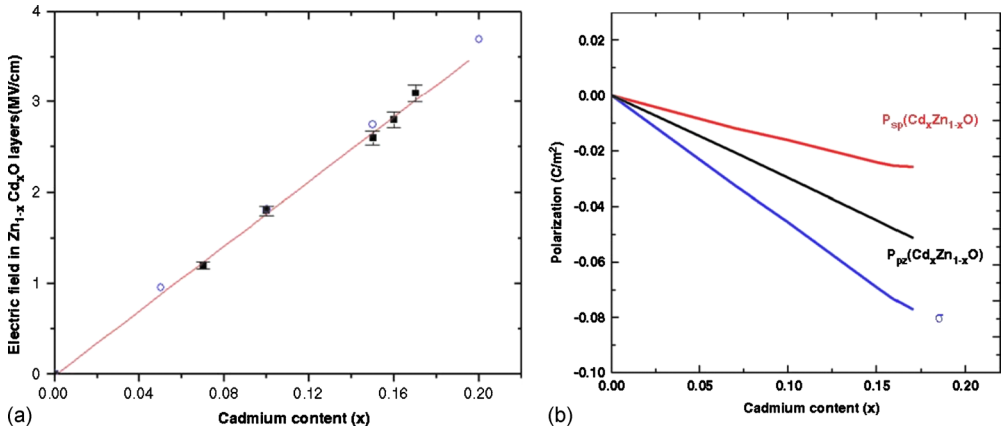

FIG. 7. (Color online) (a) Electric field (filled circles—Ref. 106, open circles—Ref. 105) and (b) polarization and charge density (σ), as a function of Cd concentration in $Cd_xZn_{1-x}O$ QWs. Reprinted with permission from F. Benharrats, K. Zitouni, A. Kadri, and B. Gil, Superlattices Microstruct. **47**, 592 (2010). ©2010, Elsevier.

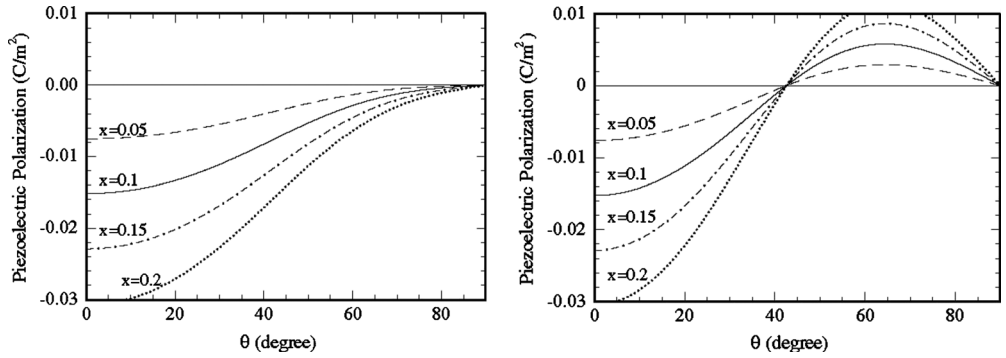

FIG. 8. Polarization field for InGaN/GaN QWs using two sets of material parameters. Reprinted with permission from M. Feneberg and K. Thonke, J. Phys.: Condens. Matter **19**, 403201 (2007). ©2007, Institute of Physics.

be zero for $(10\bar{1}0)$ orientation.[109] Experimentally, Feneberg *et al.*[110] found the internal field to be only -0.1 MV/cm for the GaInN semipolar $(1\bar{1}01)$ face but as high as -1.9 MV/cm for QWs grown on polar (0001) faces. Calculations for different angles are given in Fig. 8, illustrating the impact of different parameter sets on the angular dependence.

Details on how to model the orientation effect for QW structures will now be given, based upon the recent work of Duggen *et al.*[111] The QW is modeled as a 1D structure in z (imposing $(\partial/\partial x)=(\partial/\partial y)=0$). In order to model orientation effects due to differences in heterostructure growth and unit-cell c-axis directions, one rotates the coordinate system using two subsequent rotations as shown in Fig. 9. A rotation of this kind is described by the matrix $\mathbf{A}$ being a function of the angles ϕ,θ:

$$\mathbf{A}=\begin{bmatrix}\cos\phi & \sin\phi & 0\\ -\cos\theta\sin\phi & \cos\theta\cos\phi & \sin\theta\\ \sin\theta\sin\phi & -\sin\theta\cos\phi & \cos\theta\end{bmatrix}. \tag{41}$$

The different quantities in Eqs. (23) and (24) are then transformed by

$$\mathbf{r}'=\mathbf{A}\cdot\mathbf{r}, \tag{42}$$

$$\mathbf{T}'=\mathbf{M}\cdot\mathbf{T}, \tag{43}$$

$$\mathbf{S}'=\mathbf{N}\cdot\mathbf{S}, \tag{44}$$

$$\mathbf{E}'=\mathbf{A}\cdot\mathbf{E}, \tag{45}$$

$$\mathbf{D}'=\mathbf{A}\cdot\mathbf{D}, \tag{46}$$

$$\boldsymbol{\epsilon}'=\mathbf{A}\cdot\boldsymbol{\epsilon}\cdot\mathbf{A}^T, \tag{47}$$

$$\mathbf{e}'=\mathbf{A}\cdot\mathbf{e}\cdot\mathbf{M}^T, \tag{48}$$

$$\mathbf{c}^{\mathbf{E}\prime}=\mathbf{M}\cdot\mathbf{c}^{\mathbf{E}}\cdot\mathbf{M}^T, \tag{49}$$

where $\mathbf{r}$ denotes a position vector, the bond stress and strain transformation matrices $\mathbf{M},\mathbf{N}$ are constructed by elements of $\mathbf{a}$ as given in Ref. 6 (p. 74), and the prime indicates that the respective quantity is expressed with respect to the rotated coordinate system. Hence, the operator $\nabla\cdot$ transforms to $\nabla'\cdot$, where $\nabla'\cdot$ involves derivatives with respect to rotated coordinates. It should be noted, that the transformed parameter matrices are independent of ϕ (cylindrical symmetry) as expected.[5,96,112] From the basis vectors,

$$\hat{\mathbf{x}}'=\hat{\mathbf{x}}_\phi=\hat{\mathbf{x}}\cos\phi+\hat{\mathbf{y}}\sin\phi, \tag{50}$$

$$\hat{\mathbf{y}}'=\hat{\mathbf{y}}_\phi\cos\theta+\hat{\mathbf{z}}_\phi\sin\theta=-\hat{\mathbf{x}}\sin\phi\cos\theta+\hat{\mathbf{y}}\cos\phi\cos\theta+\hat{\mathbf{z}}\sin\theta, \tag{51}$$

$$\hat{\mathbf{z}}'=-\hat{\mathbf{y}}_\phi\sin\theta+\hat{\mathbf{z}}_\phi\cos\theta=\hat{\mathbf{x}}\sin\phi\sin\theta-\hat{\mathbf{y}}\cos\phi\sin\theta+\hat{\mathbf{z}}\cos\theta, \tag{52}$$

one observes that, as expected, $\hat{\mathbf{z}}'$ traces a sphere with center (0,0,0), such that one can model all growth directions for $0\le\phi\le2\pi$ and $0\le\theta\le\pi$. On the other hand, the $\hat{\mathbf{x}}'$ basis vector always lies in the $\hat{\mathbf{x}}\hat{\mathbf{y}}$-plane and depends on ϕ only. Thus, one expects the $S_{5'}=2S_{x'z'}$ strain component to be independent of the crystal orientation. In the following, primes are omitted for convenience (this should not lead to confusion as, henceforth, all quantities are now transformed quantities). One can write the general solution for the displacement $\mathbf{u}$ as

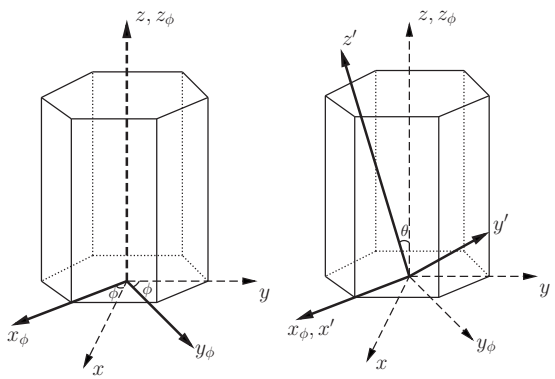

FIG. 9. Left: first rotation of angle ϕ around the z-axis. Right: second rotation of angle θ around the intermediate x_ϕ-axis. The growth direction of the heterostructure is always chosen to be along the z'-direction such that the interface planes are coplanar with the $x'y'$-plane. Reprinted with permission from L. Duggen and M. Willatzen, Phys. Rev. B **82**, 205303 (2010). ©2010, American Physical Society.

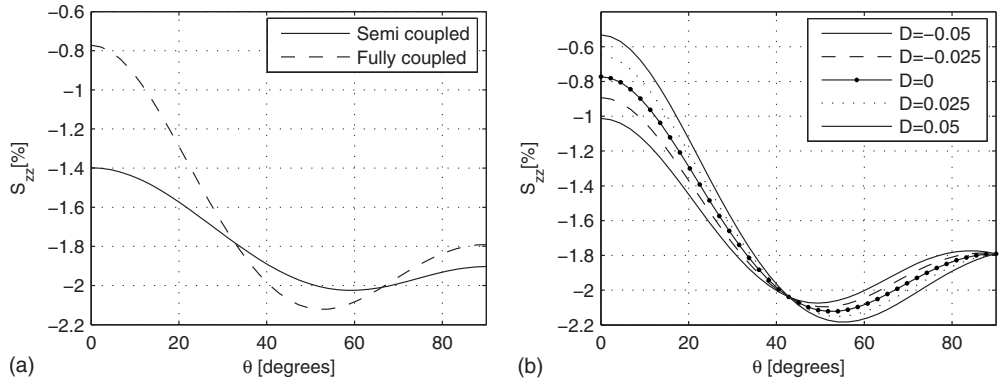

FIG. 10. Compressional strain component S_{zz} in AlN for a GaN/AlN/GaN heterostructure; (a) the fully-coupled and the semicoupled models corresponding to $D=0$ and for (b) several applied electric displacement fields D (in units of C/m^2). Reprinted with permission from L. Duggen and M. Willatzen, Phys. Rev. B **82**, 205303 (2010). ©2010, American Physical Society.

$$u_i = \begin{cases} \mathcal{A}_i^{(1)} z + \mathcal{B}_i^{(1)} & z_L \le z \le 0 \\ \mathcal{A}_i^{(2)} z + \mathcal{B}_i^{(2)} & 0 \le z \le z_1 \\ \mathcal{A}_i^{(3)} z + \mathcal{B}_i^{(3)} & z_1 \le z \le z_R \end{cases} . \tag{53}$$

The coefficients $\mathcal{A}_i$ and $\mathcal{B}_i$ can be found by mechanical and electric conditions that are continuity of

$$T_3, T_4, T_5, u_x, u_y, u_z, E_x, E_y, D_z, \tag{54}$$

everywhere. They are applied at the outer boundaries and material interfaces where, for the outer boundaries, one further assumes stress-free conditions $\mathbf{T}=0$, no transverse electric field components $E_x=E_y=0$ and $D_z=D$ where D is a known (applied) constant. To enforce $E_x=E_y=0$ throughout the whole structure, one has, from Eq. (24),

$$[\boldsymbol{\epsilon}^{(i)-1}\mathbf{D}^{(i)}]_1 = [\boldsymbol{\epsilon}^{(i)-1}\mathbf{P}^{(i)}]_1 + [\boldsymbol{\epsilon}^{(i)-1}\mathbf{e}^{(i)}\mathbf{S}^{(i)}]_1, \tag{55}$$

$$[\boldsymbol{\epsilon}^{(i)-1}\mathbf{D}^{(i)}]_2 = [\boldsymbol{\epsilon}^{(i)-1}\mathbf{P}^{(i)}]_2 + [\boldsymbol{\epsilon}^{(i)-1}\mathbf{e}^{(i)}\mathbf{S}^{(i)}]_2, \tag{56}$$

where $i=1,2,3$, such that these equations have to apply in each material layer. Inserting Eq. (24) into Eq. (23) and eliminating $\mathbf{E}$, the conditions for $\mathbf{T}$ can be expressed by the unknown $\mathcal{A}$-coefficients along with the unknown $D_x^{(i)}, D_y^{(i)}$. Together with Eqs. (55) and (56), one can solve for the strain and the electric displacement field components $D_x^{(i)}, D_y^{(i)}$. From the latter solutions, the electric-field component $E_z^{(i)}$ can be calculated using Eq. (24).

Results, using the fully-coupled and semicoupled models for GaN/AlGaN/GaN structures are shown in Figs. 10 and 11. Note that S_{xz} is always zero, since it is zero for the [0001] growth direction and, as mentioned above, independent of the growth direction. The shear strain S_{yz} have been left out because this strain is significantly smaller than the compressional strain for all growth directions. The angle θ can be linked to Miller-index notation by taking directions $[\bar{1}2\bar{1}N]$ with $N=2c/(a\tan\theta)$. Hence, $\theta=0$ corresponds to [0001], $\theta \approx 38.7°$ to $[\bar{1}2\bar{1}4]$, $\theta \approx 46.9°$ to $[\bar{1}2\bar{1}3]$, and $\theta \approx 58°$ to $[\bar{1}2\bar{1}2]$, being a cut along a crystal diagonal plane. Finally, $\theta=90°$ corresponds to $[\bar{1}2\bar{1}0]$.

One sees from Fig. 10(a) that the magnitude of the compressional strain for a [0001] growth direction changes significantly between the two models in agreement with previous findings.[63] The model differences become less significant when the growth direction changes away from [0001]. The angle of maximum compressional strain magnitude is changed by almost 10° when $D=0$ and similarly for other D-values. Also, the fully-coupled model predicts a larger change in compressional strain as one changes the growth direction. While the semicoupled model predicts a range from -1.4% to -2% (so the maximum strain magnitude being about 1.5 times as large as for the [0001] growth direction), the fully-coupled model predicts a range from -0.8% to -2.1%, the maximum strain magnitude almost

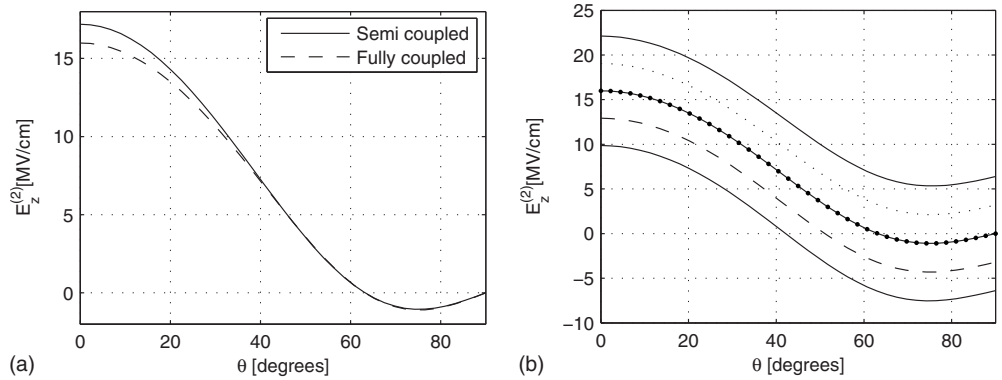

FIG. 11. Electric field component E_z in AlN for a GaN/AlN/GaN heterostructure; (a) corresponding to $D=0$ and (b) for several applied electric displacements D. The legend is the same as in Fig. 10. Reprinted with permission from L. Duggen and M. Willatzen, Phys. Rev. B **82**, 205303 (2010). ©2010, American Physical Society.

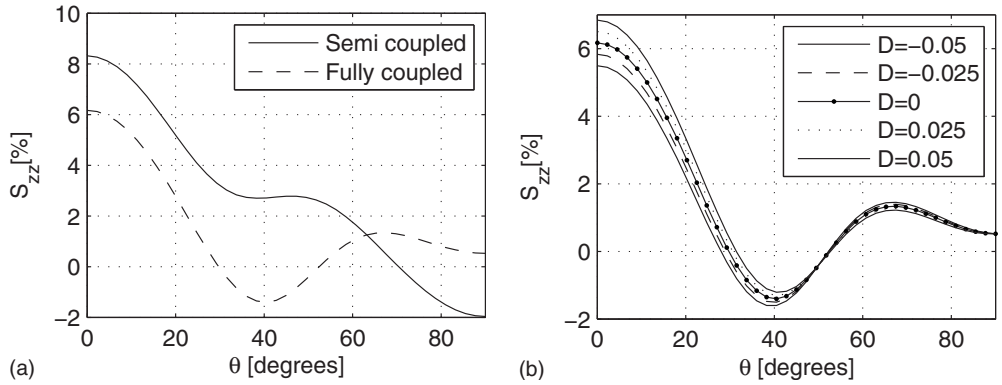

FIG. 12. Compressional strain component S_{zz} in the QW layer (ZnO/MgO/ZnO heterostructure) for (a) the fully-coupled and the semicoupled models corresponding to $D=0$ (in units of C/m^2) and for (b) several applied electric displacement fields D. Reprinted with permission from L. Duggen and M. Willatzen, Phys. Rev. B **82**, 205303 (2010). ©2010, American Physical Society.

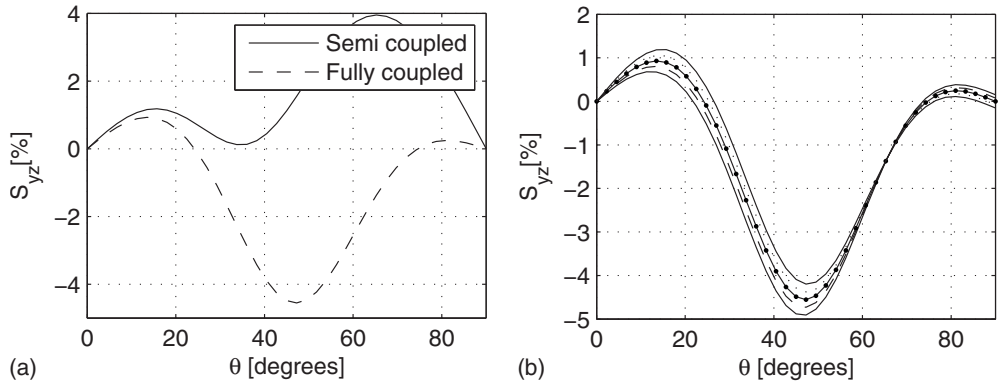

FIG. 13. Shear strain component S_{yz} in the QW layer (ZnO/MgO/ZnO heterostructure) for (a) the fully-coupled and the semicoupled models corresponding to $D=0$ and for (b) several applied electric displacement fields D. The legend is the same as in Fig. 12. Reprinted with permission from L. Duggen and M. Willatzen, Phys. Rev. B **82**, 205303 (2010). ©2010, American Physical Society.

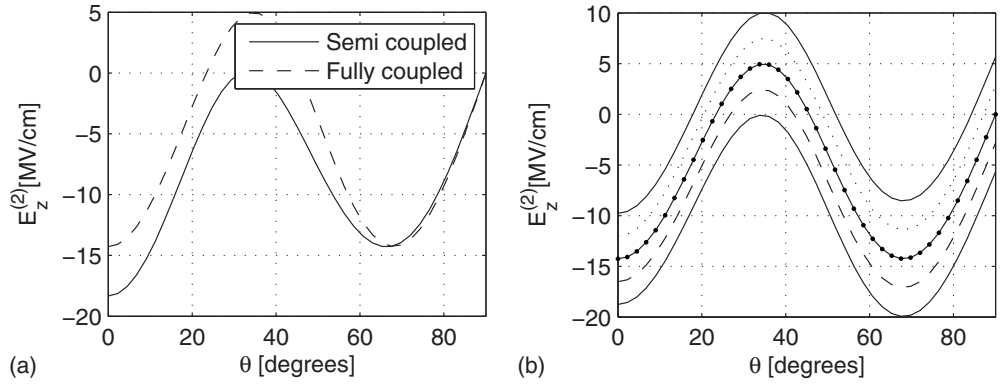

FIG. 14. Electric field component E_z in ZnMgO for a ZnO/ZnMgO/ZnO heterostructure; (a) corresponding to $D=0$ and (b) for several applied electric displacements D. The legend is the same as in Fig. 12. Reprinted with permission from L. Duggen and M. Willatzen, Phys. Rev. B **82**, 205303 (2010). ©2010, American Physical Society.

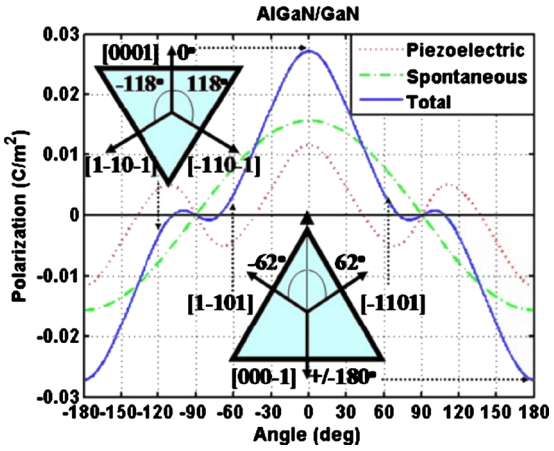

FIG. 15. (Color online) Polarization fields for a core shell $Al_{0.3}Ga_{0.7}N/GaN$ nanowire. Reprinted with permission from M. A. Mastro, B. Simpkins, G. T. Wang, J. Hite, C. R. Eddy, Jr., H.-Y. Kim, J. Ahn, and J. Kim, Nanotechnology **21**, 145205 (2010). ©2010, Institute of Physics.

three times as large as for the [0001] growth direction. Further, as one sees in Fig. 11(a), the electric field in the QW reverses direction in the interval from approximately $\theta = 65°$ to $\theta = 90°$ being zero close to $\theta = 65°$ for $D = 0$. Another interesting observation is the strain dependence on the applied electric displacement field D [Fig. 10(b)].

The corresponding results for a ZnO/MgO/ZnO QW heterostructure are shown in Figs. 12–14. As seen in Fig. 12(a), the quality of the semicoupled model for S_{zz} is in the same order of magnitude as for the nitrides. In contrast to the nitrides, one sees in Fig. 13(a), that the quality of the semicoupled model becomes much worse for the shear strain S_{yz} for $30° < \theta < 90°$, a region where the shear strain can be even larger than the compressional strain. It can be seen in Fig. 13(b) that, also for the shear strain, there is a growth direction (near $\theta = 65°$) where the shear strain does not depend on the applied electric displacement field D, hence it is independent of the applied electric potential across the heterostructure (but note that this does not appear at the same growth direction as for the compressional strain). Another interesting observation about this structure is the electric field in AlN as seen in Figs. 14(a) and 14(b) where the field reverses direction twice, such that, for several D values, there are two growth directions at which the electric field becomes zero in the central layer.

The above work emphasized the need to use a fully-coupled model in calculating optimum growth angles for different applications where strain distributions play a significant role. Also we see that the electric field in AlN shows a zero crossing when changing the growth direction thus making it possible to design a crystal where the electric field in AlN is zero even at small applied voltages.

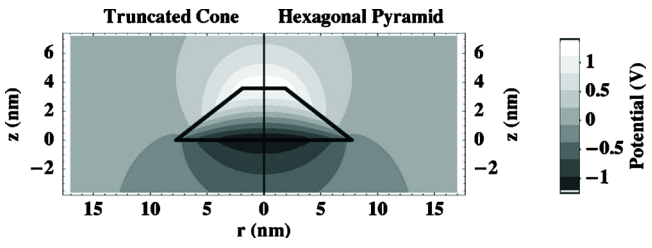

FIG. 16. (Color online) Comparison between a truncated cone and a hexagonal pyramid QD. Reprinted with permission from D. P. Williams, A. D. Andreev, E. P. O'Reilly, and D. A. Faux, Phys. Rev. B **72**, 235318 (2005). ©2005, American Physical Society.

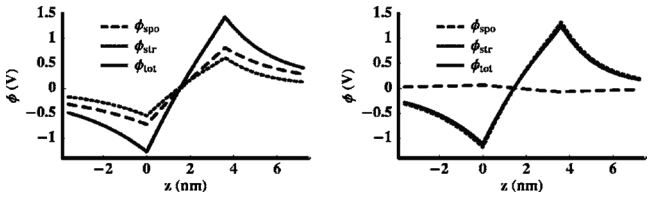

FIG. 17. Comparison of contributions to the piezoelectric potential between GaN/AlN and InN/GaN QDs. Reprinted with permission from D. P. Williams, A. D. Andreev, E. P. O'Reilly, and D. A. Faux, Phys. Rev. B **72**, 235318 (2005). ©2005, American Physical Society.

2. Quantum wires

There are fewer studies of electromechanical phenomena in quantum wires.[113–115] An example is the synthesis of dopant-free GaN/AlN/AlGaN radial nanowire heterostructures and the demonstration of the existence of an electron gas with an intrinsic electron mobility of 3100 $cm^2/V\,s$ and 21000 $cm^2/V\,s$ at room temperature and 5 K, respectively.[113] A theoretical calculation of such core-shell nanowires grown in the $[11\bar{2}0]$ direction showed that the polarization field at the {0001} facets is much larger than at the $\{1\bar{1}01\}$ facets (Fig. 15). The structures actually grown have a 152 nm GaN core on its $(000\bar{1})$ side, a 21 nm $(000\bar{1})$ AlGaN layer, and a 49 nm $\{1\bar{1}01\}$ AlGaN layer.

Knowledge of the polarization fields was used in order to design an undoped nanowire transistor that displayed *p*-type operation due to polarization-induced hole carriers at the $(000\bar{1})$ AlGaN/GaN interface.[115]

A quite different study of the electromechanical effect in ZnO nanowires was suggested by uniaxial tensile experiments that showed a softening of the Young's modulus by 30%–40% of the bulk value for nanowires of 200–400 nm.[116] Quantitative agreement was obtained using a model that linked the mechanical properties to the internal electric field. This could have an impact on the analysis of other experiments on the mechanical properties of nanostructures.

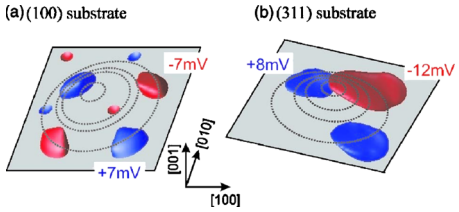

FIG. 18. (Color online) Piezoelectric potential for InAs/InP QDs (truncated cylindrical pyramids) on two different substrate orientations. Reprinted with permission from C. Cornet, A. Schliwa, J. Even, F. Doré, C. Celebi, A. Létoublon, E. Macé, C. Paranthoën, A. Simon, P. M. Koenraad, N. Bertru, D. Bimberg, and S. Loualiche, Phys. Rev. B **77**, 035312 (2006). ©2006, American Physical Society.

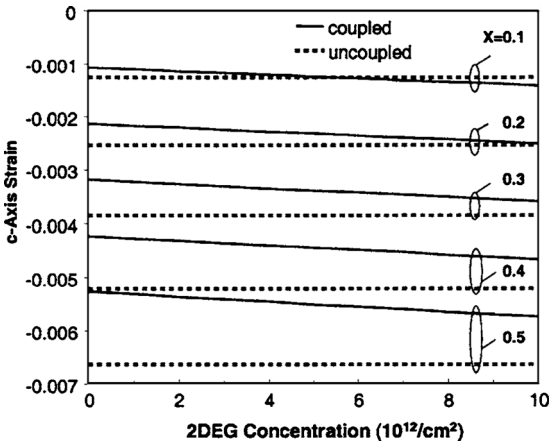

FIG. 19. *c*-axis strain calculated using fully-coupled (solid lines) and semi-coupled (dashed lines) models for $Al_xGa_{1-x}N/GaN$ as a function of the 2DEG concentration. Reprinted with permission from A. F. M. Anwar, R. T. Webster, and K. V. Smith, Appl. Phys. Lett. **88**, 203510 (2006). ©2006, American Institute of Physics.

3. QDs

Similar to QW structures, the main direct experimental consequence of the internal polarization fields is a redshift of the photoluminescence peak. This has been observed to be as big as 0.5 eV below the bulk GaN band gap for GaN/AlN QDs of average height and diameter of 4.1 and 17 nm; the piezoelectric field was estimated to be as high as 5.5 MV/cm.[117] Theoretically, piezoelectric fields in QDs have been extensively studied for WZ QDs.[81,83,84,90,91,118–125] The recent work of Schulz *et al.*[123] shows that, while the polarization field can be substantially reduced inside a QW grown along a nonpolar direction, the variety of facets of a QD grown on a nonpolar substrate means that there might not be a similar substantial reduction in the polarization field. They find that the reduction is achieved for a GaN/AlN QD, in agreement with experimental data, only if $e_{15}<0$.

GaN/AlN and InN/GaN QDs were compared by Williams *et al.*[121] Figure 16 shows that the effect of shape is negligible between a truncated cone and a hexagonal pyramid. Figure 17 shows that the contributions of spontaneous and strain-induced contributions to the potential are about equal for GaN/AlN QDs but quite different for InN/GaN QDs. Similar results have been obtained by others.[119,122]

Substrate orientation can also play a significant role on the piezoelectric effect. For example, in Fig. 18 is shown the piezoelectric potential for InAs/InP QDs (truncated cylindrical pyramids) on (100) and (311)B substrates. Both the magnitude and symmetry of the potential can be seen to be very different.

4. Influence of charge carriers on piezoelectric effects

We have seen that, in heterojunction field-effect transistors (HFETs) such as a AlN/GaN heterojunction (Fig. 5), AlN electric fields may reach several hundreds of megavolt per meter in the absence of electric charges (Fig. 20). Jogai *et al.*[60] showed that self-consistent calculations based on the Schrödinger equation and electromechanical governing equations reveal the presence of an electric charge at the AlN/GaN interface due to the difference in spontaneous polarization of the two materials (AlN and GaN) and piezoelectric effects given by:

$$e_0 n = 0.9\left[P_B^{\mathrm{sp}} - P_A^{\mathrm{sp}} + \left(2e_{31,A} - \frac{2e_{33,A}c_{13,A}}{c_{33,A}}\right)\frac{a_A - a_B}{a_A} - \frac{e_{33,A}^2}{c_{33,A}}E_A\right]. \quad (57)$$

where $A(B)$ refers to AlN (GaN), $a_A(a_B)$ is the lattice constant of AlN (GaN), and E_A is the electric field in AlN. A similar electron gas has also been verified for the ZnMgO/ZnO system.[126] The generated electric charge leads to considerably reduced electric fields (by a factor of 5–10) and hence also to a reduced influence of the electric field on strain. This, in turn, leads to a reduced difference between fully-coupled and a semicoupled model results. An example of a calculation of strain using the two different models for $Al_xGa_{1-x}N/GaN$ as a function of the two-dimensional electron gas (2DEG) concentration is given in Fig. 19.[128] In cases where a free-electron gas is not present at the heterostructure interface, however, caution must be paid in the sense that generally a full-coupled electromechanical calculation is necessary.

Nevertheless, a study on $In_{0.07}Ga_{0.93}N/GaN$ QWs showed a much smaller reduction in the internal field.[127] Thus, it was reported that carrier densities (from optical excitation) of 4.3×10^{16} m^{-2} (4.8×10^{16} m^{-2}) for 4 nm (3 nm) QWs reduce the piezoelectric field to 0.97×10^8 V m^{-1} (1.03×10^8 V m^{-1}) from a value of 1.23×10^8 V m^{-1} for the uncharged (i.e., unscreened) QWs.

5. Nonlinear effects

In the absence of free charge carriers, Fig. 20 illustrates that electric fields may be of the order of 1 GV/m such that nonlinear permittivity effects are likely to be important. Willatzen *et al.*[129] adjusted the above theory to accommodate for nonlinear-permittivity effects by using a second-order permittivity expansion in the electric field:

$$\epsilon_E = \epsilon + \epsilon_1 E + \epsilon_2 E^2, \quad (58)$$

where $\epsilon_E(\epsilon)$ is the permittivity in the presence (absence) of an electric field. For GaN, the nonlinear permittivity coefficients are:[130] $\epsilon_1=1.3\times10^{-11}\epsilon_0$ C/V^2, $\epsilon_2=15.9\times10^{-19}\epsilon_0$ C m/V^3 with $\epsilon_0=8.854\times10^{-12}$ the vacuum permittivity (note that in Fig. 20 the same values of the nonlinear permittivity coefficients: ϵ_1 and ϵ_2 were used for GaN and AlN). The results are shown in Fig. 20. In the absence of interface charge carriers, nonlinear permittivity effects lead to a reduction in the AlN electric field from approximately 1.3 to 1.1 GV/m or about 20%. However, accounting for free interface charges, shows that the additional impact of nonlinear permittivity is almost negligible and the electric field becomes approximately 0.25 GV/m whether or not nonlinear permittivity effects are considered.

Evident from the above consideration in the absence of free interface charge carriers is the strong electric fields in the AlN cap layer of AlN/GaN HFETs. It may then be speculated that electrostriction effects, i.e., second-order electric-

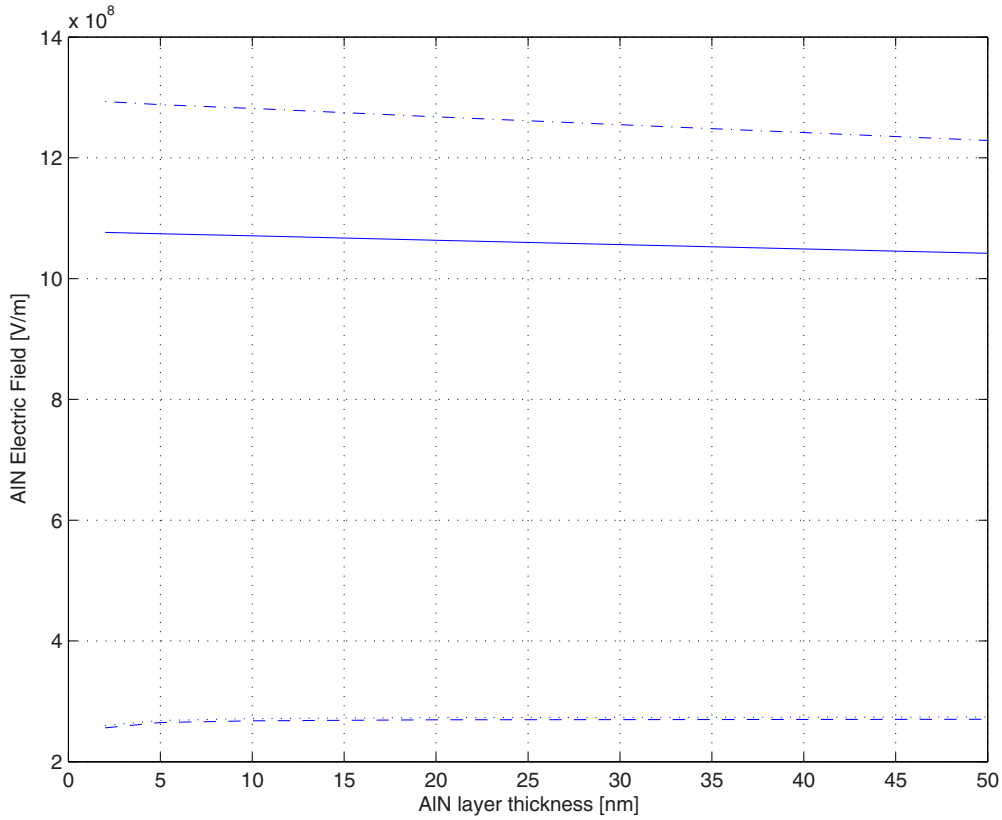

FIG. 20. (Color online) Plot of the AlN electric field vs the AlN layer thickness for an AlN film on 1 μm GaN. The (a) solid, (b) dashed-dotted, (c) long-dashed, and (d) short-dashed curves correspond to employing (a) a nonlinear permittivity without interface charges, (b) a linear permittivity without interface charges, (c) a nonlinear permittivity with interface charges, and (d) linear permittivity with interface charges. The linear model is obtained from the nonlinear model by setting the coefficients: $\epsilon_1=\epsilon_2=0$. Short-circuit voltage conditions are imposed over the full structure. Reprinted with permission from M. Willatzen, B. Lassen, and L. C. Lew Yan Voon, J. Appl. Phys. **100**, 124309 (2006). ©2006, American Institute of Physics.

field contributions to the strain become important. Note that electrostriction effects are allowed in all crystals (even in the presence of inversion symmetry) since the electrostriction coupling tensor is of rank four (even). It was experimentally argued (Ref. 58) that the electrostriction coefficient M_{zzzz} linking the strain component S_{zz} to E_z^2 is approximately three-four orders of magnitude larger as compared to similar semiconductors (e.g., AlN, MgO) and even larger than in polyvinylidene fluoride film applications where electrostriction is known to play a dominant role. Such a large electrostriction coefficient in combination with the large electric field present in GaN/AlN HFET structures (even in the presence of free charge carriers) was shown to lead to strong changes in the GaN electric field in the presence of hydrostatic pressure.[131] In actual fact, the electric field in GaN increases from nearly 0.1 to 0.2 GV/m as the hydrostatic pressure increases from 0 to 50 MPa. An even stronger impact of electrostriction was obtained for the effective GaN speed-of-sound as a function of the GaN electric field.[131] We have, however, recently carried out atomistic calculations using ABINIT (Ref. 59) that contradict the experimental result in Ref. 58. The M_{zzzz} value found in Ref. 59 for GaN (10^{-22} m^2 V^{-2}) is of the order of the experimental values reported for AlN and MgO. Hence, these recent findings suggest that even in the presence of large electric fields, electrostriction is of minor importance. Further experimental and theoretical investigations are clearly needed for electrostriction coefficient tensor values given the scarce data available in the literature so as to give a conclusive answer regarding the importance of electrostriction in WZ quantum heterostructures.

D. Piezoelectric effects on electronic band structure

We now carry the analysis further by looking at the impact of the polarization fields on the electronic properties.

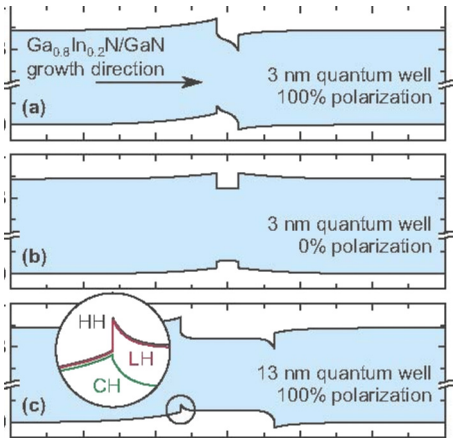

FIG. 21. (Color online) Band diagram for an (0001) $In_{0.2}Ga_{0.8}N$ QW surrounded by n-doped GaN barriers with a dopant concentration of 10^{18} cm^3. Reprinted with permission from Schubert and Schubert, Appl. Phys. Lett. **96**, 131102 (2010). ©2010, American Institute of Physics.

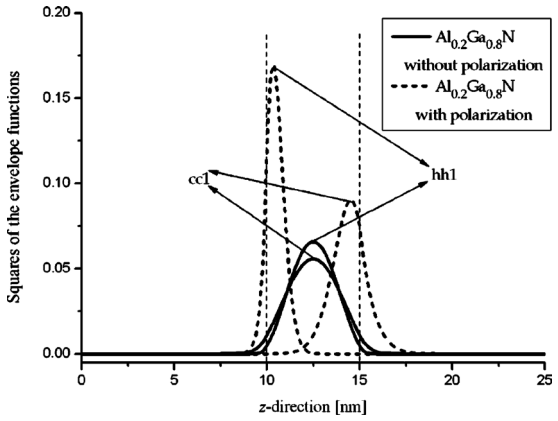

FIG. 22. Wave functions for a 5 nm GaN/$Al_{0.2}Ga_{0.8}N$ QW. The curves are without (solid) and with (dotted) polarization fields. Reprinted with permission from J. Galczak, R. P. Sarzala, and W. Nakwaski, Physics E **25**, 504 (2005). ©2005, Elsevier.

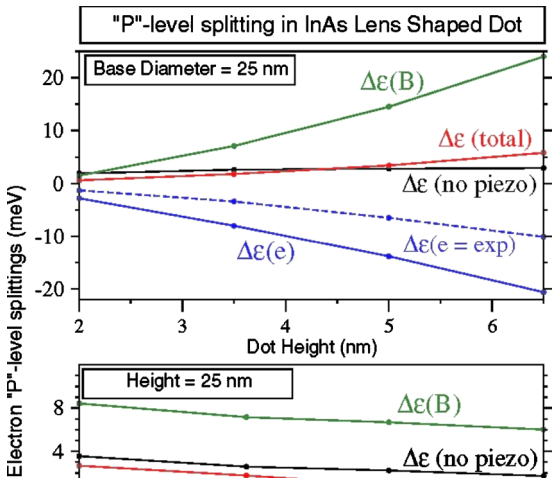

FIG. 24. (Color online) Energy splitting of *P* states for an InAs/GaAs QD. Reprinted with permission from G. Bester, A. Zunger, X. Wu, and D. Vanderbilt, Phys. Rev. B **74**, 081305(R) (2006). ©2006, American Physical Society.

1. QWs

Most of the studies here have been for WZ QWs.[60,97,98,104,106,132–137] Wang *et al.*[132] coupled the semicoupled results of Bykhovski *et al.*[96] to the Schrödinger equation and showed that, for a 50 Å GaN–$Al_{0.3}Ga_{0.7}N$ QW, the piezoelectric effect leads to a spatial separation of electron and hole wave functions. Fiorentini *et al.*[97] pointed out that a redshift in the interband transition energy can result and they included spontaneous polarization in their calculations. The origin of the redshift is the quantum-confined Stark effect due to the internal electric field. A typical band diagram is shown in Fig. 21 for an (0001) $In_{0.2}Ga_{0.8}N$ QW surrounded by *n*-doped GaN barriers with a dopant concentration of 10^{18} cm^3 (Ref. 137). An example of the reduction in overlap of the electron and hole wave functions is shown in Fig. 22. In Fig. 23, one can see the redshift in the transition energies due to the polarization fields. Also shown are experimental data and one possible explanation for them lying between the calculations with and without polarization is that the experimental data might have carrier screening effects neglected in the calculations.

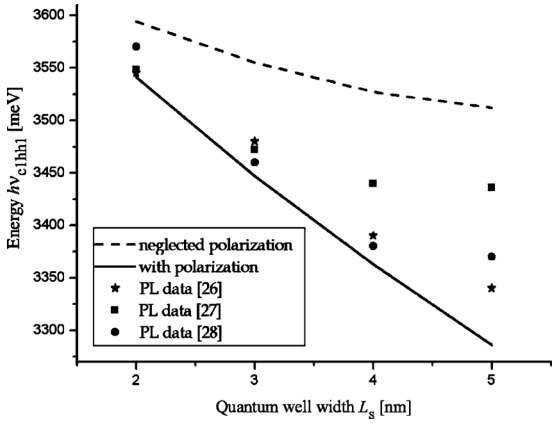

FIG. 23. Transition energy for a 5 nm GaN/$Al_{0.2}Ga_{0.8}N$ QW. The curves are without (solid) and with (dotted) polarization fields. Reprinted with permission from J. Galczak, R. P. Sarzala, and W. Nakwaski, Physica E **25**, 504 (2005). ©2005, Elsevier.

It was reported that *c*-oriented $Zn_{0.78}Mg_{0.22}O$/ZnO QWs show the quantum-confined Stark effect due to the built-in field of approximately 1 MV/cm.[136] Earlier experimental work had apparently not confirmed the presence of any significant polarization field for this system.

2. QDs

The influence of piezoelectric effects and strain on QD electronic band structures has been investigated in, e.g., Refs. 78, 80, 83–85, 90, 118–120, 122, 123, and 138. It was shown for InAs/GaAs pyramidal QDs on a wetting layer using a semicoupled piezoelectric model that the heavy-hole probability density changes significantly due to piezoelectric effects.[78] The degeneracy in the first-excited states $|100\rangle$ and $|010\rangle$ in the absence of piezoelectric effects becomes lifted when the piezoelectric effect is introduced. These results em-

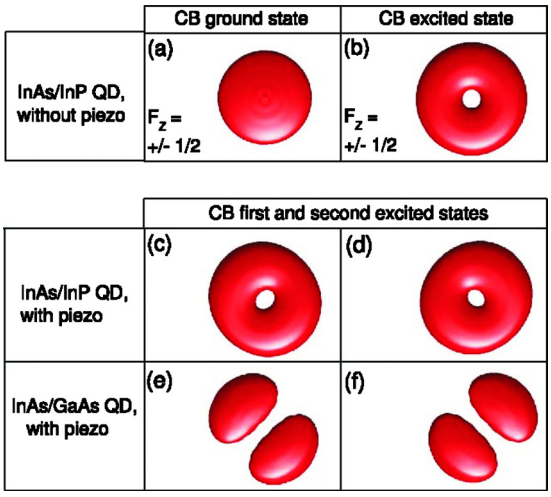

FIG. 25. (Color online) Comparison between InAs/GaAs and InAs/InP QDs. Plot is the 75% isodensity contour. Reprinted with permission from J. Even, F. Doré, C. Cornet, and L. Pedesseau, Phys. Rev. B **77**, 085305 (2008). ©2008, American Physical Society.

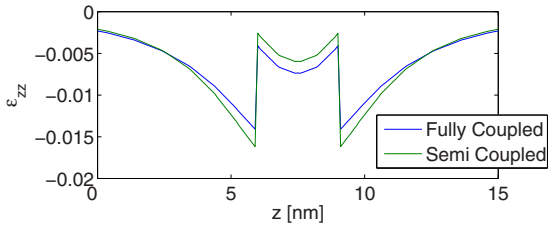

FIG. 26. (Color online) Strain component ϵ_{zz} for $r=0$ of the GaN/AlN QD. Reprinted with permission from B. Lassen, D. Barettin, M. Willatzen, and L. C. Le Yan Voon, Microelectron. J. **39**, 1226 (2008). ©2008, Elsevier.

phasize the important changes in electronic wave functions, band structure, and eventually optoelectronic properties as a consequence of piezoelectric effects.

Bester *et al.*[3] found that the linear and nonlinear piezoelectric contributions nearly cancel each other out for an InAs/GaAs QD (Fig. 24). The splitting of the electron P states (second and third electron states) has been attributed to the lower symmetry of the microscopic crystal field as opposed to the symmetry from a continuum theory, and to the piezoelectric effect. They find that the splitting, taking into account a second-order piezoelectric contribution, is reduced to only about 6 meV as opposed to about 20 meV for a lens-shaped QD of height 6.5 nm. Nevertheless, Even *et al.*[85] found that there can also be a splitting of the conduction P states of ~1 meV due to coupling to valence states, even within the continuum model.

Comparisons of the electronic states in QDs of different materials have been performed. For example, Fig. 25 is between InAs/GaAs and InAs/InP QDs. The larger piezoelectric effect for the former leads to a symmetry reduction from $C_{\infty v}$ to C_{2v}.

The impact of a fully-coupled model versus a semicoupled one has been studied by Lassen *et al.*[92] They investigated the influence of electromechanical effects on the electron structure of GaN/AlN cylindrical QDs. They found that differences in using a semicoupled and a fully-coupled model for conduction-band energies amount to 10 meV and 36 meV as the cylinder QD radius increases from approximately 4 nm to 15 nm, respectively (we note that 36 meV corresponds to the exciton binding energy in GaN/AlN); hence it is important to use a fully-coupled model for the larger-radius QDs. In Ref. 92, differences in the strain of about 30% (Fig. 26) and up to 30 meV in the electron energies were found for a GaN cylindrical QD embedded in an AlN matrix. For a dot with height $h=3$ nm and radius $R=5$ nm, the data in Table VI were obtained. Evidently, approximately 25 meV difference is found for the various conduction-band levels between a fully-coupled and a semicoupled model analysis.

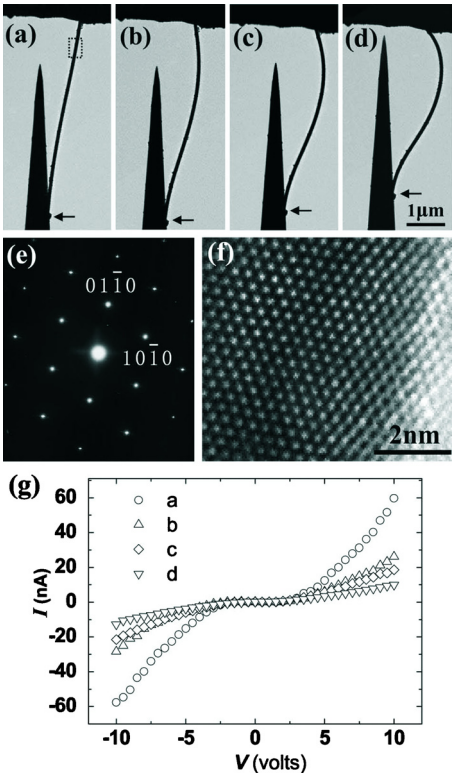

FIG. 27. (Color online) Transmission electron microscopy images and $I-V$ curves for bent ZnO nanowires. Reprinted with permission from K. H. Liu, P. Gao, Z. Xu, X. D. Bai, and E. G. Wang, Appl. Phys. Lett. **92**, 213105 (2008). ©2008, American Institute of Physics.

E. Nanopiezotronics

The term nanopiezotronics was coined by Wang's group[139,140] and they define it to be the study of the coupled piezoelectric and semiconducting properties of nanowires for electronic device applications. He has also recently coined the term piezophototronic.[141] We have decided to group together the work in this area in a separate section even though it concerns the direct effect in nanowires.

1. Experiments

At this point, most of the papers in the field of nanopiezotronics are from Wang's group.[142–160]

A number of measurements on piezoelectric nanowires have been made, but many of these measurements involved extraneous factors, such as vibration[161] and combined compressive and bending forces.[144] Wang and Song[142] bent ZnO nanowires in a nanowire array with an atomic force microscope (AFM), using a conductive tip to measure the induced voltages. This method, however, is inherently limited in how far the nanowire can be bent, both due to the presence of neighboring nanowires and because the AFM tip will slide

TABLE VI. Electron energies (eV) for a GaN/AlN QD. The zero of energy is the bulk GaN conduction-band edge. Reproduced with permission from Ref. 92.

Fully-coupled	0.194	0.273	0.374	0.498	0.660
Semicoupled	0.167	0.247	0.349	0.473	0.635
Difference	0.027	0.025	0.025	0.025	0.025

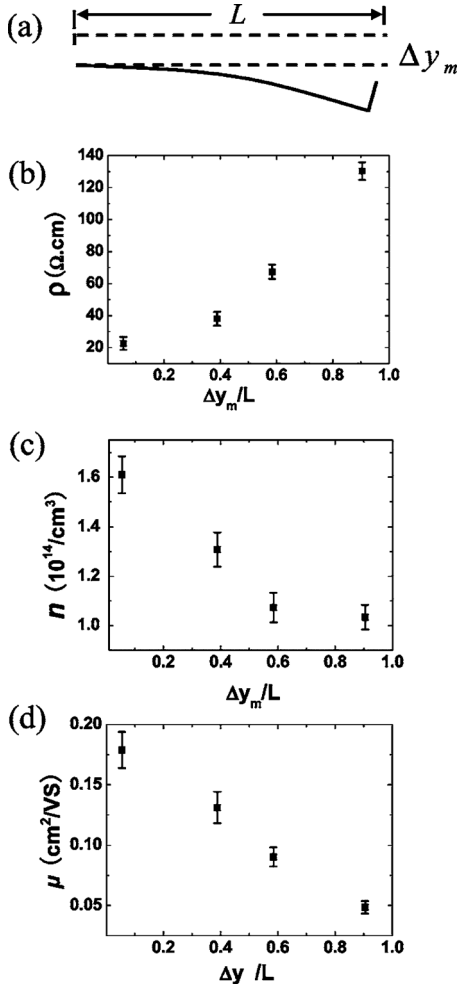

FIG. 28. Resistivity, electron concentration, and carrier mobility as a function of nanowire bending. Reprinted with permission from K. H. Liu, P. Gao, Z. Xu, X. D. Bai, and E. G. Wang, Appl. Phys. Lett. **92**, 213105 (2008). ©2008, American Institute of Physics.

off of the nanowire at a certain maximum angle of bend. Also in this configuration, a direct measurement of the degree of bending is not possible.

Liu *et al.*[155] reported an *in situ* measurement of the electrical properties ($I-V$ curves) of individual bent ZnO nanowires inside a high resolution transmission electron microscope (Fig. 27). In this fashion, they were able to obtain the resistivity, electron concentration, and carrier mobility as a function of bending (Fig. 28).

2. Theory

Theoretically, nanopiezotronics is studied using the same coupled set of electromechanical equations, Eqs. (23)–(27). For the study of piezoelectric nanogenerators through the lateral bending of nanowires, Gao and Wang[148] proposed the solution to the following set of coupled differential equations:

$$\nabla \cdot \sigma = 0, \tag{59}$$

$$\sigma_p = c_{pq}\epsilon_q - e_{kp}E_k, \tag{60}$$

$$D_i = e_{iq}\epsilon_q + \kappa_{ik}E_k, \tag{61}$$

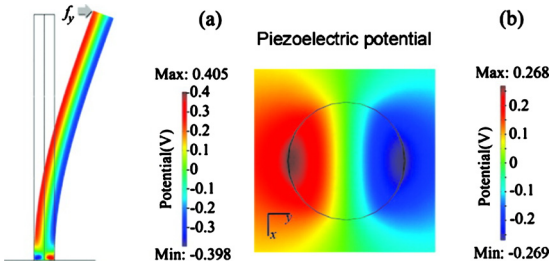

FIG. 29. (Color online) Voltage distribution for a bent nanowire. Reproduced, with permission from American Chemical Society, from Ref. 148.

$$e_{ilm}e_{jpq}\frac{\partial^2 \epsilon_{mp}}{\partial x_l \partial x_q} = 0, \tag{62}$$

$$\nabla \cdot \mathbf{D} = 0. \tag{63}$$

In the above, Eq. (59) is the mechanical equilibrium equation (static Navier) for the stress tensor, Eqs. (60) and (61) are constitutive equations with ϵ the strain tensor, κ the dielectric constant, E the electric field, and D the displacement field, Eq. (62) is the geometrical compatibility condition on the strain tensor, and Eq. (63) is the Gauss equation.

Using perturbation theory, Wang *et al.* derived a formula for the maximum voltage generated on the nanowire surface at the tensile (T) and compressive (C) sides to be[148,162]

$$V_{\max}^{(T,C)} = \pm \frac{3}{4(\kappa_0 + \kappa_\perp)}[e_{33} - 2(1+\nu)e_{15} - 2\nu e_{31}]\frac{a^3}{l^3}\nu_{\max}, \tag{64}$$

where κ_0 is the vacuum permittivity, $\kappa_\perp$ is the dielectric constant, e_{33}, e_{15}, e_{31} are the piezoelectric coefficients, ν is the Poisson ratio, a the radius, l the length, and $\nu_{\max}$ the maximum deflection. The potential distribution for a ZnO nanowire 50 nm in diameter and 600 μm in length under a lateral bending force of 80 nN is shown in Fig. 29. The maximum voltage generated is about 0.3 V; a simplified continuum model gave a similar result.[163] Another work did confirm this theoretical value of the potential,[156,157] for a similar force at a height of 300 nm; the bending they obtained is 133 nm. However, they did dispute how this would translate into an actual voltage signal. Their circuit analysis using the low capacitance of the ZnO ($\sim 4\times10^{-5}$ pF) and the resistivity of the n-doped semiconducting nanowires (1 Ωcm) would indicate that the signal should only be of the order of 10^{-10} V. They also apparently observed the effect with a Si nanowire, a nonpiezoelectric material.[157] Correspondingly, the latter work has been disputed by Wang.[158]

3. Applications

Experimentally, nanopiezotronics focuses on creating useful devices based on nano-scale piezoelectric elements, such as nanowires and nanobelts. Indeed, a number of device concepts have already been explored, such as using piezoelectric nanowires as a nanogenerator,[142] or incorporating such a nanowire into a force-detecting FET (Ref. 144) or a gated diode.[149] A GaAs-based nanoelectromechanical systems using voltage-tunably coupled piezoelectric actuation

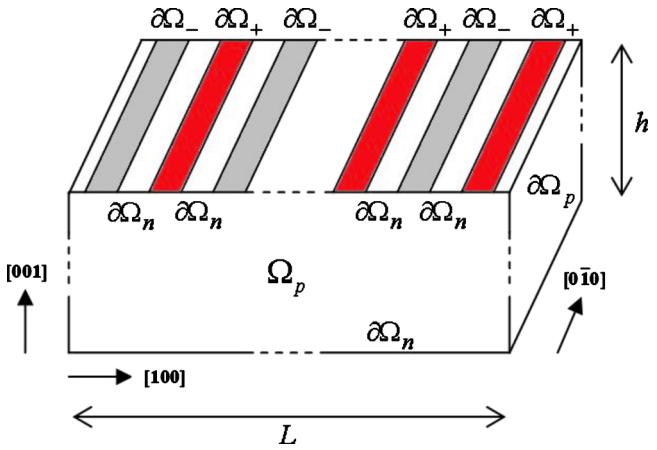

FIG. 30. (Color online) Schematic of a SAW device. Interdigital metal electrodes are placed on the upper surface (gray-black stripes). Reprinted with permission from Y. Gao and Z. L. Wang, Nano Lett. **7**, 2499 (2007). ©2007, American Chemical Society.

was recently demonstrated.[164] For small perturbations, the frequency shift in the resonance of the clamped cantilever due to an applied dc field can be written as[164]

$$\Delta f = -\sqrt{\frac{3Y}{\rho}}\frac{d_{3j}V}{2\pi t^2}, \tag{65}$$

where Y is the Young's modulus, ρ the density, t the total device thickness, and V the dc voltage.

Many of these device concepts, however, involve complex bending or bending and compression of the nanostructures in order to induce voltages, causing nonuniform strain fields within the nanowire. Similarly, in piezoelectric actuation, an electric field creates a strain which leads to a bending moment if the strain is asymmetrically distributed about the beam's neutral axis.[164] The analysis of the electromechanics within the nanowire generating the piezoelectric voltages is thus nontrivial. For completeness, we mention a recent nonlinear theory of the energy harvesting process.[159,165]

F. Surface acoustic waves (SAWs)

As an important example of nanopiezoelectric actuation, we review a SAW device following Ref. 166. SAWs are elastic waves which propagate along the surface of an elastic body while dying out exponentially into the bulk of the body. SAW devices are widely used in today's modern high frequency communication systems due to their stability and reliability even in the gigahertz region. A SAW device consists of a piezoelectric material (or film) on which interdigitated

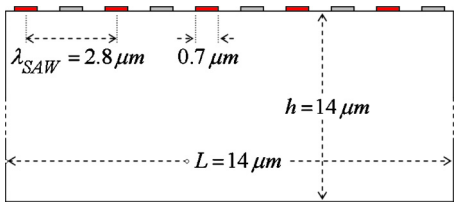

FIG. 31. (Color online) 2D-section of the SAW-device (as modeled in COMSOL MULTIPHYSICS). Reprinted with permission from D. B. Carstensen, T. Amby-Christensen, M. Willatzen, and P. V. Santos, Technical Acoustics **19**, 1 (2008). ©2008, Technical Acoustics.

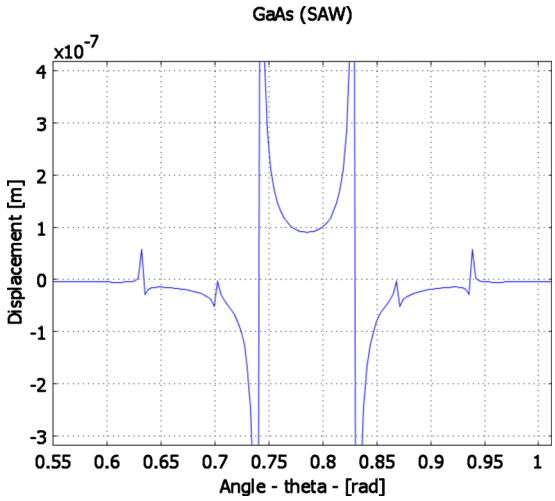

FIG. 32. (Color online) Orientation angle sweep—at constant frequency (1.022 GHz) (v-displacement). Reprinted with permission from D. B. Carstensen, T. Amby-Christensen, M. Willatzen, and P. V. Santos, Technical Acoustics **19**, 1 (2008). ©2008, Technical Acoustics.

transducers are placed (Fig. 30). Usually a single SAW device operates as an input and an output transducer. This makes it possible to create an acoustic wave by applying a voltage signal and vice versa. This property makes SAW devices interesting for applications allowing it, e.g., to operate as an analog electric filter at selected frequencies (in the range from about 10 MHz to 2.5 GHz). SAW devices are also widely used in mobile phone technology, wireless communication and telecommunication systems,[167] acoustically induced charge transport, light storage, modulation of photonic structures, optically cavities and the driving of micromechanical systems. Recent SAW applications include interaction of SAWs with electrons confined to a QW enabling an effective reduction in dimensionality but with the advantage, compared to quantum wires and QDs, that deleterious effects such as interface and size fluctuations are avoided.[168–172] Furthermore, the use of SAWs allows dynamic control of band structure and wave functions with possible applications in, e.g., optoelectronics. Quantum teleportation effected

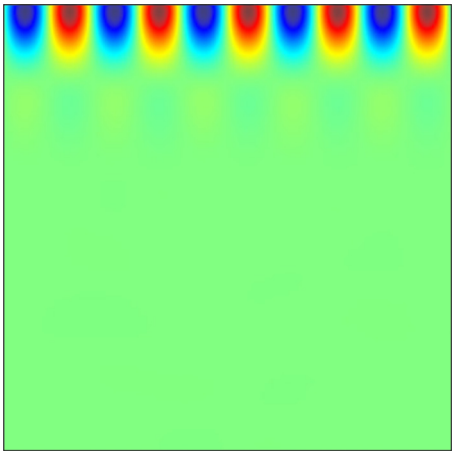

FIG. 33. (Color online) Rayleigh wave at the top surface $\theta = \pi/4$ rad, frequency equals 1.022 GHz (v-displacement). Reprinted with permission from D. B. Carstensen, T. Amby-Christensen, M. Willatzen, and P. V. Santos, Technical Acoustics **19**, 1 (2008). ©2008, Technical Acoustics.

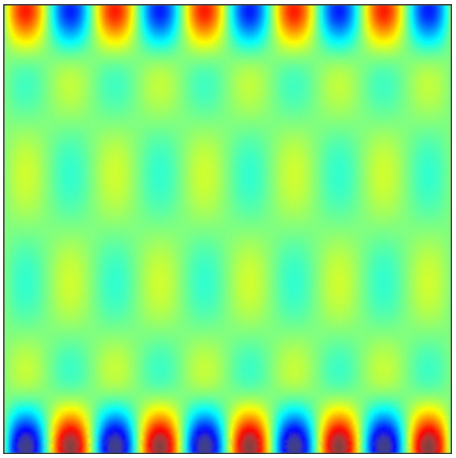

FIG. 34. (Color online) Rayleigh wave at the top and bottom surfaces for $\theta=0.632$ rad. The frequency equals 1.022 GHz (v-displacement). A similar mode is found at $\theta=0.939$ rad, however, characterized by a most significant displacement at the top surface. Reprinted with permission from D. B. Carstensen, T. Amby-Christensen, M. Willatzen, and P. V. Santos, Technical Acoustics **19**, 1 (2008). ©2008, Technical Acoustics.

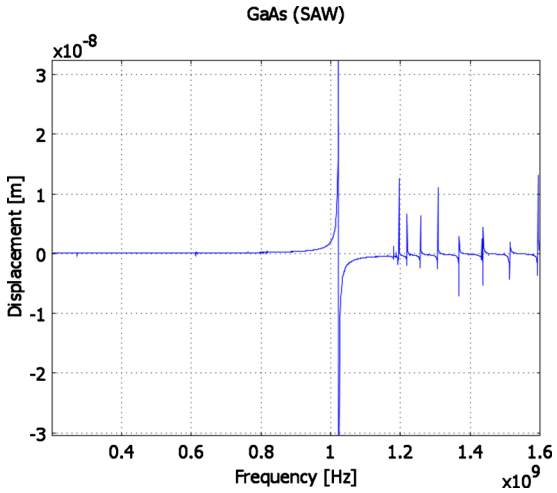

FIG. 36. (Color online) Frequency sweep fixed angle $\theta=\pi/4$ rad (v-displacement). Reprinted with permission from D. B. Carstensen, T. Amby-Christensen, M. Willatzen, and P. V. Santos, Technical Acoustics **19**, 1 (2008). ©2008, Technical Acoustics.

through SAW injection control of electrons in a network of interacting semiconductor quantum wires has also recently been investigated theoretically.[173–175] It was shown in Ref. 176 that SAWs prevent the spreading of electron wave functions and reduce undesirable reflection effects. SAWs provide new ways of exploring quantum-confined systems including conductivity and Dirac electron wave functions in graphene.[176–179]

1. Modeling results and comparison with measurements

The modeling of a SAW transducer based on GaAs will now be discussed; it allows one to determine resonance frequencies vs. rectangular macroscopic structure rotation angle with respect to the crystal axes. The model assumes no free charges in the structure and solves the Maxwell–Poisson equation together with Navier's equations for ZB (GaAs) symmetry. The modeled structure with dimensions is shown in Fig. 31. In the computations, variations along the [010] direction were neglected.

Figure 32 shows a plot of the [010] displacement (denoted v in the following) for different values of the rotation angle θ at a fixed frequency (rotation around the [001] axis). It can clearly be seen that there exists a symmetry around the rotation angle $\pi/4$ ($\theta=\pi/4$ is equivalent to the [110] direction). At this angle and in the vicinity of it, a Rayleigh wave is generated. In actual fact, a double resonance with respect to rotation angle is found near $\pi/4$.

Figure 33 shows the Rayleigh wave deformation at the top surface of the model corresponding to the rotation angle $\theta=\pi/4$. Away from the symmetry point ($\theta=\pi/4$), other resonance frequencies are found. The resonance frequencies near 0.632 and 0.939 rad (symmetric angles with respect to $\pi/4$) correspond to Rayleigh waves with significant displacements at the top- and the bottom surfaces, respectively.

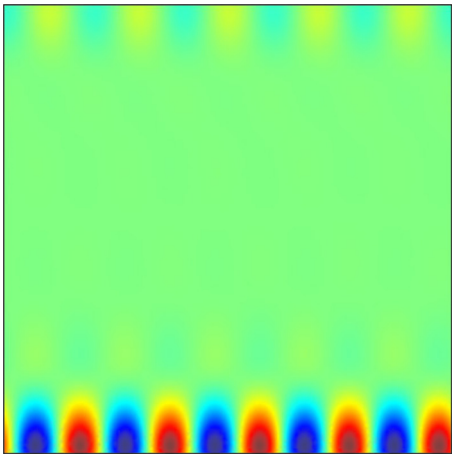

FIG. 35. (Color online) Rayleigh wave at the bottom surface corresponding to $\theta=0.703$ rad and the frequency equals 1.022 GHz (v-displacement). Reprinted with permission from D. B. Carstensen, T. Amby-Christensen, M. Willatzen, and P. V. Santos, Technical Acoustics **19**, 1 (2008). ©2008, Technical Acoustics.

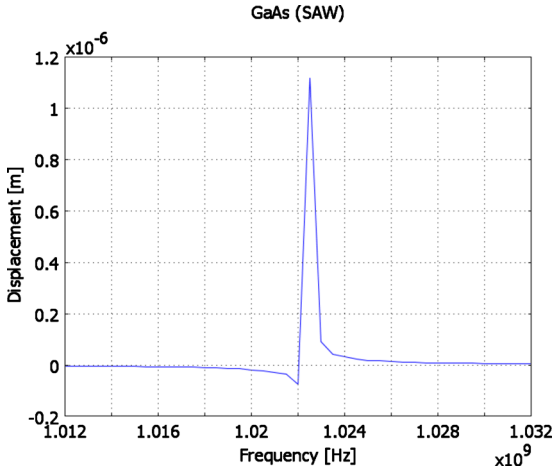

FIG. 37. (Color online) Frequency sweep near 1.022 GHz for a fixed rotation angle: $\theta=\pi/4$ rad (v-displacement). Reprinted with permission from D. B. Carstensen, T. Amby-Christensen, M. Willatzen, and P. V. Santos, Technical Acoustics **19**, 1 (2008). ©2008, Technical Acoustics.

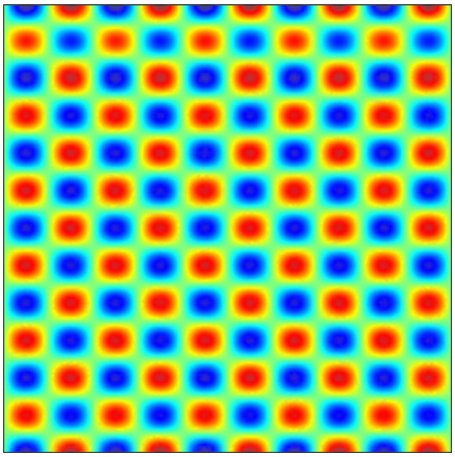

FIG. 38. (Color online) Lamb wave at a frequency of 1.512 GHz. The rotation angle θ is $\pi/4$ rad (v-displacement). Reprinted with permission from D. B. Carstensen, T. Amby-Christensen, M. Willatzen, and P. V. Santos, Technical Acoustics **19**, 1 (2008). ©2008, Technical Acoustics.

We emphasize that the displacement amplitudes of these two Rayleigh waves are considerably smaller than the one found near $\pi/4$.

Figure 34 shows Rayleigh waves generated at the top and bottom surfaces at an orientation angle $\theta=0.939$ rad. The resonance frequencies found near 0.703 and 0.868 rad (again symmetric angles around $\pi/4$) correspond to Rayleigh waves at the bottom surface. Again, it was found that the maximum amplitude of the displacement v is smaller than the one found at $\pi/4$. In Fig. 35, a Rayleigh wave at the bottom of the device is shown corresponding to $\theta=0.703$ rad.

For any rotation angle, the SAW device has several resonance frequencies. A sweep in the frequency from 100 MHz to 1.6 GHz for a SAW structure with $\theta=\pi/4$ reveals[166] a number of resonance frequencies (Fig. 36). The one near 1.022 GHz gives the strongest deformation. Figure 37 shows a plot of the displacement v near 1.022 GHz.

A substantial part of the other resonance frequencies (those above 1.1 GHz) corresponds to Lamb waves [where strong deformations exist across the structure and not only at the top or bottom surface(s)]. Figure 38 shows such a Lamb wave deformation.

The resonance frequency of 1.022 GHz calculated by Carstensen *et al.* is in excellent agreement with measurements carried out by de Lima, Jr. *et al.*[180,181] where they examined a device with similar parameters. For completeness, we note that, in Ref. 166, zero-stress boundary conditions were imposed at the top boundary. As an example of a different boundary condition, in Ref. 182, results for a single-electroded SAW device were presented based on the material system lithium niobate $LiNbO_3$) where Neumann boundary conditions are imposed for the displacement and electric potential at the top surface while the lower surface is subject to Dirichlet boundary conditions. Not surprisingly, the results in Ref. 182 are somewhat different as compared to Ref. 166, due to the different material choices and differences in the boundary conditions.

IV. SUMMARY

We have provided a review of electromechanical effects in semiconductor nanostructures. We hope to have convinced the reader that the study of the effects in such materials and structures have revealed a number of new understandings but also open questions. In particular,

- The ZB and WZ semiconductors are interesting electromechanical materials due to relatively large piezoelectric constants and, in the WZ case, spontaneous polarization. The piezoelectric constants can be positive and negative. Nevertheless, there is still a wide discrepancy among experimental and among theoretical values of most electromechanical coefficients. For example, even the sign of e_{15} for WZ materials remains undetermined.
- The most visible consequences of electromechanical effects in semiconducting heterostructures are the quantum-confined Stark effect, whereby the transition energies are redshifted and the optical transitions are weakened, and the generation of a voltage difference when the heterostructures are bent.
- The piezoelectric properties of WZ nanomaterials depend strongly on the interplay between the strained-induced piezoelectric field and the spontaneous polarization. In general, one can expect polarization as large as 10^{-2} C/m^2, electric fields of the order of 1 MV/cm, and changes in the electronic energies as high as hundreds of millielectron volt. In particular, everything else being the same, the electric field increases from ZnMgO/ZnO to ZnCdO/ZnO to AlGaN/GaN QWs.
- The polarization field inside nanostructures depends upon the orientation due to the anisotropic piezoelectric coefficients. Different coefficients currently found in the literature can, unfortunately, give very different angular dependence including the existence or not of a zero-field angle. This is a serious limitation since the design of QW lasers on different facets is a topic of great current interest.
- The importance of nonlinear effects has not been fully ascertained. For example, *ab initio* calculations seem to indicate that second-order piezoelectric coefficients might be important; yet, experimental data for InGaAs/GaAs QW can be explained using a nonlinear strain model as well. Experimentally, there is one report of a large electrostrictive effect in GaN; nevertheless, *ab initio* calculations indicate otherwise. Finally, nonlinearity has not been considered in the bending of nanowires. Hence, much research remains to be done in this area.
- Fully-coupled models for the effects are generally required for quantitative accuracy for WZ nanostructures but can be ignored for traditional ZB ones. However, in the presence of screening charges, semicoupled models work quite well even for WZ nanostructures.
- There is some disagreement as to whether the current theory of nanopiezotronics really explains the experimental results on voltage generation. Competing theories give voltages differing by nine orders of magni-

tude. Nevertheless, vibrations of the nanowires have led to energy generation in the nJ range.

- The use of SAW devices in nanotechnology is ever-increasing as it allows for tuning electronic wave functions and energy gaps so as to optimize transport properties and dynamic optical properties in different applications.

ACKNOWLEDGMENTS

L.C.L.Y.V. would like to thank Sønderborg Kommune and the Air Force Office of Scientific Research (AFOSR) for funding some of the work reported in this review article, and the Mads Clausen Institute for their hospitality during the initial stages of writing the article. We are grateful to Dr. Benny Lassen for the cover image.

[1]W. G. Cady, *Piezoelectricity*, 1st ed. (McGraw-Hill, New York, 1946).
[2]G. Bester, X. Wu, D. Vanderbilt, and A. Zunger, Phys. Rev. Lett. **96**, 187602 (2006).
[3]G. Bester, A. Zunger, X. Wu, and D. Vanderbilt, Phys. Rev. B **74**, 081305(R) (2006).
[4]R. E. Newnham, V. Sundar, R. Yimnirun, J. Su, and Q. M. Zhang, J. Phys. Chem. B **101**, 10141 (1997).
[5]L. D. Landau and E. M. Lifshitz, *Theory of Elasticity*, Course of Theoretical Physics, Vol. 7, 3rd ed. (Butterworth–Heinemann, Oxford, 1999).
[6]B. A. Auld, *Acoustic Fields and Waves in Solids* (Pergamon, New York, 1990), Vol. 1–2.
[7]D. Berlincourt, H. Jaffe, and L. R. Shiozawa, Phys. Rev. **129**, 1009 (1963).
[8]P. Maheswaranathan, R. J. Sladek, and U. Debska, Phys. Rev. B **31**, 7910 (1985).
[9]S. Muensit, E. M. Goldys, and I. L. Guy, Appl. Phys. Lett. **75**, 3965 (1999).
[10]I. L. Guy, S. Muensit, and E. M. Goldys, Appl. Phys. Lett. **75**, 4133 (1999).
[11]M.-H. Zhao, Z.-L. Wang, and S. X. Mao, Nano Lett. **4**, 587 (2004).
[12]H. J. Fan, W. Lee, R. Hauschild, M. Alexe, G. L. Rhun, R. Scholz, A. Dadgar, K. Nielsch, H. Kalt, A. Krost, M. Zacharias, and U. Gösele, Small **2**, 561 (2006).
[13]D. A. Scrymgeour, T. L. Sounart, N. C. Simmons, and J. W. P. Hsu, J. Appl. Phys. **101**, 014316 (2007).
[14]V. Tilak, P. Batoni, J. Jiang, and A. Knobloch, Appl. Phys. Lett. **90**, 043508 (2007).
[15]F. Felten, G. A. Schneider, J. M. Saldana, and S. V. Kalinin, J. Appl. Phys. **96**, 563 (2004).
[16]S. V. Kalinin, E. A. Eliseev, and A. N. Morozovska, Appl. Phys. Lett. **88**, 232904 (2006).
[17]A. N. Morozovska, S. V. Svechnikov, E. A. Eliseev, and S. V. Kalinin, Phys. Rev. B **76**, 054123 (2007).
[18]T. Jungk, A. Hoffmann, and E. Soergel, Appl. Phys. Lett. **91**, 253511 (2007).
[19]I. Mahboob, K. Nishiguchi, A. Fujiwara, and H. Yamaguchi, Appl. Phys. Lett. **95**, 233102 (2009).
[20]M. Feneberg and K. Thonke, J. Phys.: Condens. Matter **19**, 403201 (2007).
[21]M. Born, *Dynamik der Kristallgitter* (Teubner, Leipzig, 1915).
[22]M. Born and E. Bormann, Ann. Phys. **62**, 218 (1920).
[23]M. Born and M. Göppert-Mayer, *Handbuch der Physik* (Verlag Julius Springer, Berlin, 1933), Vol. 24, Chap. 4, p. 635.
[24]M. Born, *Problems of Atomic Dynamics* (Frederick Ungar, New York, 1960).
[25]K. Huang, Philos. Mag. **40**, 733 (1949).
[26]M. Born and K. Huang, *Dynamical Theory of Crystal Lattices* (Oxford University Press, Oxford, 1954).
[27]J. L. Birman, Phys. Rev. **111**, 1510 (1958).
[28]J. C. Phillips and J. A. Van Vechten, Phys. Rev. Lett. **23**, 1115 (1969).
[29]J. W. F. Woo, Phys. Rev. B **4**, 1218 (1971).
[30]T. Hidaka, Phys. Rev. B **5**, 4030 (1972).
[31]R. M. Martin, Phys. Rev. B **5**, 1607 (1972).
[32]W. A. Harrison, Phys. Rev. B **10**, 767 (1974).
[33]H.-c. Hwang and J. H. Henkel, Phys. Rev. B **17**, 4100 (1978).
[34]K.-s. Kam and J. H. Henkel, Phys. Rev. B **17**, 1361 (1978).
[35]S. Y. Ren, Phys. Rev. B **22**, 2908 (1980).
[36]J. B. McKitterick, Phys. Rev. B **28**, 7384 (1983).
[37]S. de Gironcoli, S. Baroni, and R. Resta, Phys. Rev. Lett. **62**, 2853 (1989).
[38]A. Dal Corso, R. Resta, and S. Baroni, Phys. Rev. B **47**, 16252 (1993).
[39]A. Dal Corso, M. Posternak, R. Resta, and A. Baldereschi, Phys. Rev. B **50**, 10715 (1994).
[40]A. P. Mirgorodsky, M. B. Smirnov, E. Abdelmounîm, T. Merle, and P. E. Quintard, Phys. Rev. B **52**, 3993 (1995).
[41]F. Bernardini, V. Fiorentini, and D. Vanderbilt, Phys. Rev. B **56**, R10024 (1997).
[42]K. Shimada, T. Sota, and K. Suzuki, J. Appl. Phys. **84**, 4951 (1998).
[43]F. Bernardini and V. Fiorentini, Phys. Rev. B **64**, 085207 (2001).
[44]F. Bernardini and V. Fiorentini, Appl. Phys. Lett. **80**, 4145 (2002).
[45]Y. Noel, M. Llunell, R. Orlando, P. D'Arco, and R. Dovesi, Phys. Rev. B **66**, 214107 (2002).
[46]X. Wu, D. Vanderbilt, and D. R. Hamann, Phys. Rev. B **72**, 035105 (2005).
[47]P. Gopal and N. A. Spaldin, J. Electron. Mater. **35**, 538 (2006).
[48]Z. C. Tu and X. Hu, Phys. Rev. B **74**, 035434 (2006).
[49]W. A. Harrison, Phys. Rev. B **74**, 205101 (2006).
[50]Y. Zheng, E. Shi, J. Chen, T. Zhang, and L. Song, J. Phys.: Conf. Ser. **29**, 61 (2006).
[51]J. Xin, Y. Zheng, and E. Shi, Appl. Phys. Lett. **91**, 112902 (2007).
[52]F. Tasnádi, B. Alling, C. Höglund, G. Wingqvist, J. Birch, L. Hultman, and I. A. Abrikosov, Phys. Rev. Lett. **104**, 137601 (2010).
[53]R. D. King-Smith and D. Vanderbilt, Phys. Rev. B **47**, 1651 (1993).
[54]M. A. Migliorato, D. Powell, A. G. Cullis, T. Hammerschmidt, and G. P. Srivastava, Phys. Rev. B **74**, 245332 (2006).
[55]R. Garg, A. Hüe, V. Haxha, M. A. Migliorato, T. Hammerschmidt, and G. P. Srivastava, Appl. Phys. Lett. **95**, 041912 (2009).
[56]J. Even, F. Dorë, C. Cornet, L. Pedesseau, A. Schliwa, and D. Bimberg, Appl. Phys. Lett. **91**, 122112 (2007).
[57]S. W. P. van Sterkenburg, J. Phys. D: Appl. Phys. **25**, 996 (1992).
[58]I. L. Guy, S. Muensit, and E. M. Goldys, Appl. Phys. Lett. **75**, 3641 (1999).
[59]I. Kornev, M. Willatzen, B. Lassen, and L. C. Lew Yan Voon, AIP Conf. Proc. **1199**, 71 (2010).
[60]B. Jogai, J. D. Albrecht, and E. Pan, J. Appl. Phys. **94**, 3984 (2003).
[61]B. Jogai, J. D. Albrecht, and E. Pan, J. Appl. Phys. **94**, 6566 (2003).
[62]U. M. E. Christmas, A. D. Andreev, and D. A. Faux, J. Appl. Phys. **98**, 073522 (2005).
[63]M. Willatzen, B. Lassen, L. C. Lew Yan Voon, and R. Melnik, J. Appl. Phys. **100**, 024302 (2006).
[64]D. L. Smith, Solid State Commun. **57**, 919 (1986).
[65]D. L. Smith and C. Mailhiot, J. Appl. Phys. **63**, 2717 (1988).
[66]J. Cibert, R. André, C. Bodin, L. S. Dang, G. Feuillet, and P. H. Jouneau, Phys. Scr. **1993**, 487 (1993).
[67]L. Duggen, M. Willatzen, and B. Lassen, Phys. Rev. B **78**, 205323 (2008).
[68]E. Caridi, T. Chang, K. Goossen, and L. Eastman, Appl. Phys. Lett. **56**, 659 (1990).
[69]J. I. Izpura, J. Sánchez, J. Sánchez-Rojas, and E. Muñoz, Microelectron. J. **30**, 439 (1999).
[70]P. Ballet, P. Disseix, J. Leymarie, A. Vasson, A.-M. Vasson, and R. Grey, Phys. Rev. B **59**, R5308 (1999).
[71]R. A. Hogg, T. A. Fisher, A. R. K. Willcox, D. M. Whittaker, M. S. Skolnick, D. J. Mowbray, J. P. R. David, A. S. Pabla, G. J. Rees, R. Grey, J. Woodhead, J. L. Sanchez-Rojas, G. Hill, M. A. Pate, and P. N. Robson, Phys. Rev. B **48**, 8491 (1993).
[72]J. L. Sánchez-Rojas, A. Sacedón, F. González-Sanz, E. Calleja, and E. Muñoz, Appl. Phys. Lett. **65**, 2042 (1994).
[73]C. H. Chan, M. C. Chen, H. H. Lin, Y. F. Chen, G. J. Jan, and Y. H. Chen, Appl. Phys. Lett. **72**, 1208 (1998).
[74]S. Cho, A. Majerfeld, A. Sanz-Hervás, J. J. Sánchez, J. L. Sánchez-Rojas, and I. Izpura, J. Appl. Phys. **90**, 915 (2001).
[75]S. Cho, J. Kim, A. Sanz-Hervás, A. Majerfeld, G. Patriarche, and B. W. Kim, Phys. Status Solidi A **195**, 260 (2003).
[76]S. Cho, A. Sanz-Hervás, J. Kim, A. Majerfeld, and B. W. Kim, J. Appl. Phys. **96**, 1909 (2004).
[77]S. P. Łepkowski, Phys. Rev. B **77**, 155327 (2008).
[78]M. Grundmann, O. Stier, and D. Bimberg, Phys. Rev. B **52**, 11969 (1995).
[79]J. H. Davies, J. Appl. Phys. **84**, 1358 (1998).
[80]O. Stier, M. Grundmann, and D. Bimberg, Phys. Rev. B **59**, 5688 (1999).
[81]E. Pan, J. Appl. Phys. **91**, 3785 (2002).

[82] E. Pan, J. Appl. Phys. **91**, 6379 (2002).
[83] T. Saito and Y. Arakawa, Physica E **15**, 169 (2002).
[84] S. Schulz, S. Schumacher, and G. Czycholl, Phys. Rev. B **73**, 245327 (2006).
[85] J. Even, F. Doré, C. Cornet, and L. Pedesseau, Phys. Rev. B **77**, 085305 (2008).
[86] T. O. Cheche and Y.-C. Chang, J. Appl. Phys. **104**, 083524 (2008).
[87] Z. Wei, Y. Zhong-Yuan, and L. Yu-Min, Chin. Phys. B **19**, 067302 (2010).
[88] S. B. Healy and E. P. O'Reilly, J. Phys.: Conf. Ser. **245**, 012022 (2010).
[89] B. Lassen, M. Willatzen, D. Barettin, R. V. N. Melnik, and L. C. Lew Yan Voon, J. Phys.: Conf. Ser. **107**, 012008 (2008).
[90] A. D. Andreev and E. P. O'Reilly, Phys. Rev. B **62**, 15851 (2000).
[91] E. O. Melezhik and O. A. Korotchenkov, J. Appl. Phys. **102**, 013503 (2007).
[92] B. Lassen, D. Barettin, M. Willatzen, and L. C. Lew Yan Voon, Microelectron. J. **39**, 1226 (2008).
[93] T. Takeuchi, S. Sota, M. Katsuragawa, M. Komori, H. Takeuchi, H. Amano, and I. Akasaki, Jpn. J. Appl. Phys., Part 2 **36**, L382 (1997).
[94] J. Seo Im, H. Kollmer, J. Off, A. Sohmer, F. Scholz, and A. Hangleiter, Phys. Rev. B **57**, R9435 (1998).
[95] G. Martin, A. Botchkarev, A. Rockett, and H. Morkoc, Appl. Phys. Lett. **68**, 2541 (1996).
[96] A. Bykhovski, B. Gelmont, and M. Shur, J. Appl. Phys. **74**, 6734 (1993).
[97] V. Fiorentini, F. Bernardini, F. Della Sala, A. Di Carlo, and P. Lugli, Phys. Rev. B **60**, 8849 (1999).
[98] J. Galczak, R. P. Sarzala, and W. Nakwaski, Physica E **25**, 504 (2005).
[99] D. Balaz, K. Kalna, M. Kuball, M. J. Uren, and A. Asenov, Phys. Status Solidi C **6**, S1007 (2009).
[100] I. P. Ipatova, V. G. Malyshkin, and V. A. Shchukin, J. Appl. Phys. **74**, 7198 (1993).
[101] L. C. Lew Yan Voon, M. Willatzen, B. Lassen, and R. Melnik, Proceedings of International Symposium on Advanced Dielectric Materials and Electronic Devices, (Cincinnati, 2006 Vol. 1), p. 631.
[102] T. Makino, Y. Segawa, A. Ohtomo, K. Tamura, T. Yasuda, M. Kawasaki, and H. Koinuma, Appl. Phys. Lett. **79**, 1282 (2001).
[103] T. Makino, K. Tamura, C. H. Chia, Y. Segawa, M. Kawasaki, A. Ohtomo, and H. Koinuma, Appl. Phys. Lett. **81**, 2355 (2002).
[104] C. Morhain, T. Bretagnon, P. Lefebvre, X. Tang, P. Valvin, T. Guillet, B. Gil, T. Taliercio, M. Teisseire-Doninelli, B. Vinter, and C. Deparis, Phys. Rev. B **72**, 241305 (2005).
[105] S.-H. Park and D. Ahn, Appl. Phys. Lett. **94**, 083507 (2009).
[106] F. Benharrats, K. Zitouni, A. Kadri, and B. Gil, Superlattices Microstruct. **47**, 592 (2010).
[107] S. Sadofev, S. Kalusniak, J. Puls, P. Schäfer, S. Blumstengel, and F. Henneberger, Appl. Phys. Lett. **91**, 231103 (2007).
[108] T. Bretagnon, P. Lefebvre, T. Guillet, T. Taliercio, B. Gil, and C. Morhain, Appl. Phys. Lett. **90**, 201912 (2007).
[109] S.-H. Park and D. Ahn, Appl. Phys. Lett. **90**, 013505 (2007).
[110] M. Feneberg, F. Lipski, R. Sauer, K. Thonke, T. Wunderer, B. Neubert, P. Brückner, and F. Scholz, Appl. Phys. Lett. **89**, 242112 (2006).
[111] L. Duggen and M. Willatzen, Phys. Rev. B **82**, 205303 (2010).
[112] C.-N. Chen, S.-H. Chang, M.-L. Hung, J.-C. Chiang, I. Lo, W.-T. Wang, M.-H. Gau, H.-F. Kao, and M.-E. Lee, J. Appl. Phys. **101**, 043104 (2007).
[113] Y. Li, J. Xiang, F. Qian, S. Gradeak, Y. Wu, H. Yan, D. A. Blom, and C. M. Lieber, Nano Lett. **6**, 1468 (2006).
[114] G. Morello, F. Della Sala, L. Carbone, L. Manna, G. Maruccio, R. Cingolani, and M. De Giorgi, Phys. Rev. B **78**, 195313 (2008).
[115] M. A. Mastro, B. Simpkins, G. T. Wang, J. Hite, C. R. Eddy, Jr., H.-Y. Kim, J. Ahn, and J. Kim, Nanotechnology **21**, 145205 (2010).
[116] A. V. Desai and M. A. Haque, Appl. Phys. Lett. **91**, 183106 (2007).
[117] F. Widmann, J. Simon, B. Daudin, G. Feuillet, J. L. Rouvière, N. T. Pelekanos, and G. Fishman, Phys. Rev. B **58**, R15989 (1998).
[118] A. D. Andreev and E. P. OReilly, Physica E, **10**, 553 (2001).
[119] V. A. Fonoberov and A. A. Balandin, J. Appl. Phys. **94**, 7178 (2003).
[120] V. A. Fonoberov and A. A. Balandin, J. Vac. Sci. Technol. **22**, 2190 (2004).
[121] D. P. Williams, A. D. Andreev, E. P. O'Reilly, and D. A. Faux, Phys. Rev. B **72**, 235318 (2005).
[122] M. Winkelnkemper, A. Schliwa, and D. Bimberg, Phys. Rev. B **74**, 155322 (2006).
[123] S. Schulz, A. Berube, and E. P. O'Reilly, Phys. Rev. B **79**, 081401 (2009).
[124] O. Marquardt, T. Hickel, and J. Neugebauer, J. Appl. Phys. **106**, 083707 (2009).
[125] J. Even, Appl. Phys. Lett. **94**, 102105 (2009).
[126] H. Tampo, H. Shibata, K. Maejima, A. Yamada, K. Matsubara, P. Fons, S. Kashiwaya, S. Niki, Y. Chiba, T. Wakamatsu, and H. Kanie, Appl. Phys. Lett. **93**, 202104 (2008).
[127] I. Brown, P. Blood, P. Smowton, J. Thomson, S. Olaizola, A. Fox, P. Parbrook, and W. Chow, IEEE J. Quantum Electron. **42**, 1202 (2006).
[128] A. F. M. Anwar, R. T. Webster, and K. V. Smith, Appl. Phys. Lett. **88**, 203510 (2006).
[129] M. Willatzen, B. Lassen, and L. C. Lew Yan Voon, J. Appl. Phys. **100**, 124309 (2006).
[130] C.-K. Sun, S.-W. Chu, S.-P. Tai, S. Keller, U. K. Mishra, and S. P. DenBaars, Appl. Phys. Lett. **77**, 2331 (2000).
[131] M. Willatzen, L. Wang, and L. C. Lew Yan Voon, Superlattices Microstruct. **43**, 436 (2008).
[132] J. Wang, J. B. Jeon, Y. M. Sirenko, and K. W. Kim, IEEE Photonics Technol. Lett. **9**, 728 (1997).
[133] O. Ambacher, B. Foutz, J. Smart, J. R. Shealy, N. G. Weimann, K. Chu, M. Murphy, A. J. Sierakowski, W. J. Schaff, L. F. Eastman, R. Dimitrov, A. Mitchell, and M. Stutzmann, J. Appl. Phys. **87**, 334 (2000).
[134] S.-H. Park and S.-L. Chuang, J. Appl. Phys. **87**, 353 (2000).
[135] B. Jogai, J. Appl. Phys. **91**, 3721 (2002).
[136] C. Morhain, X. Tang, M. Teisseire-Doninelli, B. Lo, M. Laügt, J.-M. Chauveau, B. Vinter, O. Tottereau, P. Vennéguès, C. Deparis, and G. Neu, Superlattices Microstruct. **38**, 455 (2005).
[137] M. F. Schubert and E. F. Schubert, Appl. Phys. Lett. **96**, 131102 (2010).
[138] C. Cornet, A. Schliwa, J. Even, F. Doré, C. Celebi, A. Létoublon, E. Macé, C. Paranthoën, A. Simon, P. M. Koenraad, N. Bertru, D. Bimberg, and S. Loualiche, Phys. Rev. B **74**, 035312 (2006).
[139] Z. L. Wang, Mater. Today **10**, 20 (2007).
[140] Z. L. Wang, Adv. Mater. **19**, 889 (2007).
[141] Z. L. Wang, J. Phys. Chem. Lett. **1**, 1388 (2010).
[142] Z. L. Wang and J. Song, Science **312**, 242 (2006).
[143] J. Song, J. Zhou, and Z. L. Wang, Nano Lett. **6**, 1656 (2006).
[144] X. Wang, J. Song, J. Liu, and Z. L. Wang, Nano Lett. **6**, 2768 (2006).
[145] X. Wang, J. Song, J. Liu, and Z. L. Wang, Science **316**, 102 (2007).
[146] J. X. Cao, X. G. Gong, and R. Q. Wu, Phys. Rev. B **75**, 233302 (2007).
[147] P. Gao, J. Song, J. Liu, and Z. Wang, Adv. Mater. **19**, 67 (2007).
[148] Y. Gao and Z. L. Wang, Nano Lett. **7**, 2499 (2007).
[149] J. He, C. Hsin, J. Liu, L. Chen, and Z. Wang, Adv. Mater. **19**, 781 (2007).
[150] C. S. Lao, Q. Kuang, Z. L. Wang, M.-C. Park, and Y. Deng, Appl. Phys. Lett. **90**, 262107 (2007).
[151] C. Li, W. Guo, Y. Kong, and H. Gao, Appl. Phys. Lett. **90**, 033108 (2007).
[152] W. S. Su, Y. F. Chen, C. L. Hsiao, and L. W. Tu, Appl. Phys. Lett. **90**, 063110 (2007).
[153] S. Wang, K. H. Lam, C. L. Sun, K. W. Kwok, H. L. W. Chan, M. S. Guo, and X.-Z. Zhao, Appl. Phys. Lett. **90**, 113506 (2007).
[154] Y.-F. Lin, J. Song, Y. Ding, S.-Y. Lu, and Z. L. Wang, Appl. Phys. Lett. **92**, 022105 (2008).
[155] K. H. Liu, P. Gao, Z. Xu, X. D. Bai, and E. G. Wang, Appl. Phys. Lett. **92**, 213105 (2008).
[156] M. A. Schubert, S. Senz, M. Alexe, D. Hesse, and U. Gösele, Appl. Phys. Lett. **92**, 122904 (2008).
[157] M. Alexe, S. Senz, M. A. Schubert, D. Hesse, and U. Gösele, Adv. Mater. **20**, 4021 (2008).
[158] Z. L. Wang, Adv. Mater. **21**, 1311 (2009).
[159] F. Cottone, H. Vocca, and L. Gammaitoni, Phys. Rev. Lett. **102**, 080601 (2009).
[160] S. Xu, Y. Qin, C. Xu, Y. Wei, R. Yang, and Z. L. Wang, Nat. Nanotechnol. **5**, 366 (2010).
[161] J. Zhou, Z. Wang, A. Grots, and X. He, Solid State Commun. **144**, 118 (2007).
[162] Z. L. Wang, X. Wang, J. Song, J. Liu, and Y. Gao, IEEE Pervasive Comput. **7**, 49 (2008).
[163] Z. Z. Shao, L. Y. Wen, D. M. Wu, X. F. Wang, X. A. Zhang, and S. L. Chang, J. Phys. D: Appl. Phys. **43**, 245403 (2010).
[164] S. C. Masmanidis, R. B. Karabalin, I. D. Vlaminck, G. Borghs, M. R. Freeman, and M. L. Roukes, Science **317**, 780 (2007).
[165] L. Gammaitoni, I. Neri, and H. Vocca, Appl. Phys. Lett. **94**, 164102 (2009).
[166] D. B. Carstensen, T. Amby-Christensen, M. Willatzen, and P. V. Santos, J. Phys. Chem. Lett. **19**, 1 (2008).
[167] C. K. Campbell, *Surface Acoustic Wave Devices for Mobile and Wireless Communications* (Academic, San Diego, 1998).

[168] T. Sogawa, H. Sanada, H. Gotoh, H. Yamaguchi, S. Miyashita, and P. V. Santos, Phys. Rev. B **80**, 075304 (2009).
[169] J. M. Shilton, V. I. Talyanskii, M. Pepper, D. A. Ritchie, J. E. F. Frost, C. J. B. Ford, C. G. Smith, and G. A. C. Jones, J. Phys.: Condens. Matter **8**, L531 (1996).
[170] C. Rocke, S. Zimmermann, A. Wixforth, J. P. Kotthaus, G. Böhm, and G. Weimann, Phys. Rev. Lett. **78**, 4099 (1997).
[171] T. Sogawa, P. V. Santos, S. K. Zhang, S. Eshlaghi, A. D. Wieck, and K. H. Ploog, Phys. Rev. Lett. **87**, 276601 (2001).
[172] G. Giavaras, Phys. Rev. B **81**, 073302 (2010).
[173] F. Buscemi, P. Bordone, and A. Bertoni, Phys. Rev. B **81**, 045312 (2010).
[174] R. Rodriquez, D. K. L. Oi, M. Kataoka, C. H. W. Barnes, T. Ohshima, and A. K. Ekert, Phys. Rev. B **72**, 085329 (2005).
[175] C. H. W. Barnes, J. M. Shilton, and A. M. Robinson, Phys. Rev. B **62**, 8410 (2000).
[176] P. Thalmeier, B. Dóra, and K. Ziegler, Phys. Rev. B **81**, 041409(R) (2010).
[177] B. Luthi, *Physical Acoustics in the Solid State* (Springer, Berlin, 2004).
[178] A. Wixforth, J. P. Kotthaus, and G. Weimann, Phys. Rev. Lett. **56**, 2104 (1986).
[179] R. L. Willett, M. A. Paalanen, R. R. Ruel, K. W. West, L. N. Pfeiffer, and D. J. Bishop, Phys. Rev. Lett. **65**, 112 (1990).
[180] M. M. de Lima, W. Seidel, F. Alsina, and P. V. Santos, J. Appl. Phys. **94**, 7848 (2003).
[181] M. M. de Lima, W. Seidel, H. Kostial, and P. V. Santos, J. Appl. Phys. **96**, 3494 (2004).
[182] A. Gantner, "Mathematical modeling and numerical simulation of piezoelectrical agitated surface acoustic waves," Ph.D. thesis, University of Augsburg, 2005.